

Thanks to co-Editor for your review. Here is our point-to-point reply.

Concerning responses to R1:

R1 comment #1: “They attribute these model differences to differences in 1) pH-dependent wet deposition of NH_4^+ , 2) nitrate formation on the surface of sea salt and dust aerosol, and 3) the nitrate coarse mode fraction. They find that nitrate production on sea salt and dust is important to include in models as it tends to dominate nitrate production and controls its partitioning between the fine and coarse mode. In that sense, it seems to me that 2 and 3 above are referring to the same process.”

Author’s response: “We intend to separate discussion of section 5.2 and 5.3 because the nitrate formation on the surface of sea salt and dust aerosol (section 5.3) is important, but not the only factor, to determining nitrate size distribution (section 5.2). Also, the former focuses more on chemical process and the later on physical process and climate implication.” I find that the authors did not address the reviewer’s concern. The formation of nitrate on coarse mode dust and sea salt particles is the major factor controlling the size distribution and the ratio of coarse/total particulate nitrate in models. This is not clearly explained in the manuscript, and should be clarified in section 5.

Authors’ response: we added on lines 691-695 “Coarse mode aerosol nitrate is formed due to presence of dust and/or sea salt. In other words, the formation of nitrate on coarse mode dust and sea salt particles is the major factor controlling the size distribution. Other factors, such as $\text{NH}_3/\text{NH}_4^+/\text{NO}_3^-$ chemistry and atmospheric transport and removal processes, also affect nitrate size distribution.”

R1 comment #2: Authors did not address the reviewer’s concern “What the authors are referring to by the use of “heterogeneous chemistry” is what I would call thermodynamic partitioning between the gas and aerosol phase.” I agree with the reviewer that the use of the heterogeneous chemistry should not be applied to refer to the gas-particle thermodynamic partitioning. It is unclear in the revised manuscript whether the models are treating the formation of coarse mode nitrate by a heterogeneous uptake of HNO_3 onto dust and sea-salt particles or by an equilibrium approach. This must be clarified.

Authors’ response: On lines 225-227, we state “Please note that the heterogeneous chemical production of particulate nitrate mentioned in this paper refers only to the first order loss reaction of HNO_3 on the surface of dust and sea salt particles.” On lines 279-285, we indicate that there are two ways to account for the contribution of dust and sea salt to nitrate formation. Some models (EMAC, Oslo-CTM3, and Oslo-CTM2) include dust and/or sea salt components in their TEQM models directly (marked as TEQM in table 1 under column “How do CHEMDUSS”), while some models (EMEP, GISS-OMA, GMI, and INCA) use an approach of first order loss rate outside their TEQMs to account for the heterogeneous reactions of HNO_3 on the surface of dust and sea salt (marked as HETCHEM in table 1).

We have gone through the paper to clarify “heterogeneous chemistry”, see lines 34-35, 222, 226-227, and 826.

Concerning responses to R2:

In the added text please change the 1st sentence to: “Our work presents an initial effort to assess

nitrate simulation from chemical and physical processes (deposition).” You should be more specific by what chemical and physical processes you have looked at. And please have the rest of the paragraph corrected for English.

Author’s response: Changed the sentence to “Our work presents a first effort to assess nitrate simulation from chemical (e.g. chemistry among NH_3 , NH_4^+ , NO_3^- , SO_4^{2-} , dust and sea salt) and physical processes (e.g emission, dry deposition, and wet deposition).” The whole paragraph has been revised for English.

Why would you want to compromise the accuracy and efficiency, this sentence is misleading (line 619: “Several approximations, therefore, have been developed to compromise accuracy and efficiency.”) Is this what you meant: “Several approximations have been developed to allow computational efficiency although they might compromise the model accuracy.” Please reword.

Author’s response: Done as suggested.

Additional comments:

1) The confusion about the use of the “nitrate” term:

It should be clearly stated in the title that the paper is evaluating the particulate nitrate: “Investigation of global particulate nitrate from the AeroCom Phase III experiment.”

Instead of using nitrate aerosol it would be preferable to use particulate nitrate when referring to the particle phase as aerosol term refers to both gas and particulate fraction that are in equilibrium.

Author’s response: Done as suggested.

Line 122: Is this particulate or gas-phase nitrate: “If fixed Nr is deposited as nitrate in forests,..”

Authors’ response: Nr (Reactive nitrogen) is a term used for a variety of nitrogen compounds that support growth directly or indirectly. Nr includes the gases nitrogen oxides (NO_x), ammonia (NH_3), nitrous oxide (N_2O), as well as gas and particulate nitrate (NO_3^-). I added an explanation “including gas and particulate NO_3^- and other nitrogen compounds” in lines 124-125.

2) As mentioned by R1, N_2O_5 hydrolysis is an important heterogeneous reaction when investigating the nitrate budgets that is typically included in global models. It should be clearly stated in Table 1 or 2 and in the paper how this reaction is treated and if it is included. And some discussion on the uncertainty due to this reaction and references should be added in the manuscript.

Authors’ response: We added a column “ N_2O_5 hydrolysis” in table 1. We also added these sentences in lines 209-215.

“Meanwhile, all models consider N_2O_5 hydrolysis, the conversion of N_2O_5 to HNO_3 . The first order loss reaction occurs on the surface of tropospheric aerosols and assumes irreversible instant reaction. However, the models differ in N_2O_5 hydrolysis by considering the reaction on the surface of different aerosol types. Uptake coefficients (aka gamma factors) also differ in their relationship to temperature and RH. CHASER model is special as it allows N_2O_5 conversion to HNO_3 on liquid cloud particles. Please refer to Table 1 and the listed references for details.”

3) Add “relative” Line 78: More importantly, the relative importance of aerosol nitrate

Authors’ response: Done.

4) Add “particulate” Line 102: First, the formation of particulate nitrate,
Authors’ response: Done.

5) Given that coarse mode nitrate measurements are sparse, please include measurements that have been done in Paris during the ESQUIF campaign that found that the coarse nitrate fraction represents up to 60% of total particulate nitrate mass during the night and 80% during the day. See either Figure 13c of “Hodzic et al., ACP 2006 Aerosol chemical and optical properties over the Paris area within ESQUIF project”, or Figure 6 of Hodzic et al, AE 2006: A model evaluation of coarse-mode nitrate heterogeneous formation on dust particles.”

Authors’ response: A sentence has been added on lines 746-748: “Measurements taken in Paris during the ESQUIF campaign found that the coarse nitrate fraction represents up to 60% of the total particulate nitrate mass at night and 80% at day (Hodzic et al., 2006a, 2006b).”

6) Clarify what you mean by feedback in this sentence: Line 202: “All models use full gas phase O₃-NO_x-HO_x chemistry to produce HNO₃ and consider the feedback of nitrate aerosol formation on HNO₃ calculation.” Do you mean radiative feedbacks on photolysis or changes in the HNO₃ concentrations due to the gas/particle equilibrium?

Authors’ response: We added an explanation on lines 208-209: “changes in HNO₃ concentrations due to the gas/particle equilibrium).”

Investigation of global **particulate nitrate** from the AeroCom Phase III experiment

Formatted: Font: (Default) Times New Roman, Bold

Huisheng Bian^{1,2}, Mian Chin², Didier A. Hauglustaine³, Michael Schulz⁴, Gunnar Myhre^{5,6}, Susanne E. Bauer^{7,8}, Marianne T. Lund⁶, Vlassis A. Karydis⁹, Tom L. Kucsera¹⁰, Xiaohua Pan¹¹, Andrea Pozzer⁹, Ragnhild B. Skeie⁶, Stephen D. Steenrod¹⁰, Kengo Sudo¹², Kostas Tsigaridis^{7,8}, Alexandra P. Tsimpidi⁹, and Svetlana G. Tsyro⁴

¹ Joint Center for Environmental Technology UMBC, Baltimore, MD, USA

² Laboratory for Atmospheres, NASA Goddard Space Flight Center, Greenbelt, MD, USA

³ Laboratoire des Sciences du Climat et de l'Environnement (LSCE), UMR8212, CEA-CNRS-UVSQ, Gif-sur-Yvette, France

⁴ Norwegian Meteorological Institute, Blindern, Norway

⁵ Department of Geosciences, University of Oslo, Oslo, Norway

⁶ Center for International Climate and Environmental Research-Oslo, Oslo, Norway

⁷ The Earth Institute, Center for Climate Systems Research, Columbia University, New York, USA

⁸ NASA Goddard Institute for Space Studies, New York, USA

⁹ Max Planck Institute for Chemistry, 55128 Mainz, Germany

¹⁰ Universities Space Research Association, GESTAR, Columbia, MD, USA

¹¹ School of Computer, Mathematical and Natural Sciences, Morgan State University, Baltimore, MD, USA

¹² Center for Climate System Research, University of Tokyo, Tokyo, Japan.

Abstract

An assessment of global particulate nitrate and ammonium aerosol based on simulations from nine models participating in the AeroCom Phase III study is presented. A budget analyses was conducted to understand the typical magnitude, distribution, and diversity of the aerosols and their precursors among the models. To gain confidence on model performance, the model results were evaluated with various observations globally, including ground station measurements over North America, Europe, and East Asia for tracer concentrations and dry and wet depositions, as well as with aircraft measurements in the Northern Hemisphere mid-high latitudes for tracer vertical distributions. Given the unique chemical and physical features of the nitrate occurrence, we further investigated the similarity and differentiation among the models by examining: 1) the pH-dependent NH_3 wet deposition; 2) the nitrate formation via heterogeneous chemistry on the surface of dust and sea-salt particles **or thermodynamic equilibrium calculation including dust and sea salt ions**; and 3) the nitrate coarse mode fraction (i.e., coarse/total). It is found that HNO_3 , which is simulated explicitly based on full O_3 - HO_x - NO_x -aerosol chemistry by all models, differs by up to a factor of 9 among the models in its global tropospheric burden. This partially contributes to a large difference in NO_3^- , whose atmospheric burden differs by up to a factor of 13. The atmospheric burdens of NH_3 and NH_4^+ differ by 17 and 4, respectively. Analyses at the process level show that the large diversity in atmospheric burdens of NO_3^- , NH_3 , and NH_4^+ is also related to deposition processes. Wet deposition seems to be the dominant process in determining the diversity in NH_3 and NH_4^+ lifetimes. It is critical to correctly account for contributions of heterogeneous chemical production of nitrate on dust and sea-salt, because this process overwhelmingly controls atmospheric nitrate production (typically >80%) and determines the coarse and fine mode distribution of nitrate aerosol.

1. Introduction

49 Atmospheric aerosols adversely affect human health and play an important role in
50 changing the Earth's climate. A series of multimodel studies have been coordinated by
51 the international activity of Aerosol Comparisons between Observations and Models
52 (AeroCom) in its Phase I and II model experiments that have systematically assessed the
53 presence and influence of almost all major atmospheric anthropogenic and natural
54 aerosols (such as sulfate, dust, and carbonaceous aerosols) (e.g., Kinne et al., 2006;
55 Schulz et al., 2006; Textor et al., 2006; Koch et al., 2009; Huneus et al., 2011; Tsigaridis
56 et al., 2014; Kim et al., 2015). Very little attention has been drawn to nitrate aerosol
57 (hereafter "nitrate" referring to particulate nitrate unless otherwise specified) other than
58 its contribution to radiative forcing (Myhre et al., 2013). One obvious reason is that not
59 many models used to include nitrate owing to the chemical complexity of nitrate
60 formation. However, atmospheric nitrate aerosol not only exerts direct effects on air
61 quality and climate, but also uniquely impacts the Earth system by being directly
62 involved in tropospheric chemistry and constraining net primary productivity, hence
63 altering carbon sequestration and ecological effects, via its deposition (Prentice et al.,
64 2001).

65
66 Atmospheric nitrate contributes notably to total aerosol mass in the present-day,
67 especially in urban areas and agriculture regions. Nitrate is about a quarter of sulfate in
68 terms of overall global burden, AOD, and direct forcing at the present-day according to
69 the study of AeroCom II direct forcing experiment (Myhre et al., 2013). This conclusion
70 is confirmed by recent publications using various individual models and emission
71 inventories (Bellouin et al; 2011; Bauer et al., 2007; Hauglustaine 2014; Karydis et al.,
72 2016; Mezuman et al., 2016; Paulot et al., 2016). Regionally, considerable evidences
73 from in-situ measurements (Bessagnet et al., 2014; Haywood et al., 2008; Jimenez et al.,
74 2009; Malm et al., 1994; Vieno et al., 2016) and model results (Karydis et al., 2011;
75 Ensberg et al., 2013; Trump et al., 2015) indicate that nitrate becomes one of the major
76 aerosol species in urban and agriculture environments. For example, nitrate concentration
77 is about half of sulfate during the summer season in Beijing (Zhou et al., 2016) and
78 represents a large portion of wintertime aerosol mass in the San Joaquin Valley in
79 California (Pusede et al., 2016).

80
81 | More importantly, the **relative** importance of aerosol nitrate is likely to increase over the
82 century with a projected decline in SO₂ and NO_x emissions and increase in NH₃
83 emissions (IPCC, 2013). With the reduction of SO₂ emissions, less atmospheric NH₃ is
84 required to neutralize the strong acid H₂SO₄. The excess of NH₃ results in gaseous HNO₃
85 and NH₃ entering the condensed phase, and their subsequent dissociation yields nitrate
86 and ammonium ions. The trend of future nitrate depends on which is the limited species,
87 NO_x or NH₃, for nitrate formation (Tsimpidi et al., 2007; 2008). Generally, our
88 atmosphere, at its current and foreseeable near future, is still in an NH₃-limited condition
89 according to sensitivity studies by Heald et al. (2012) and Walker et al. (2012). Almost
90 all global models predicted an overall increase of atmospheric nitrate burden during this
91 century based on current available emission inventories (Bauer et al 2007; 2016; Bellouin
92 et al., 2011; Hauglustaine et al., 2014; Li et al., 2014). For example, using CMIP5 future
93 emission projections, Bellouin et al. (2011) concluded that, by 2090, nitrate would
94 become an important aerosol species in Europe and Asia, contributing up to two thirds of

95 the globally averaged anthropogenic optical depth. However, the predicted trend of
96 surface nitrate is mixed. Some studies estimated a consistent increase of surface nitrate
97 (Bellouin et al., 2011), while others pointed out that this increase might vanish or even
98 reverse over some regional urban areas due to the decline of NO_x emissions (Bauer et al.,
99 2016; Pusede et al., 2016; Trail et al., 2014). Nevertheless, the potentially increasing
100 importance of nitrate in climate and its large uncertainty in future surface nitrate
101 predictions urge us to characterize model performance and understand the
102 physicochemical mechanisms behind the diversity of nitrate simulations.
103

104 Nitrate is also important in that its formation directly affects tropospheric chemistry.
105 First, the formation of particulate nitrate, through either aqueous phase chemical reaction
106 between HNO_3 and NH_3 (Metzger et al., 2002; Kim et al., 1993) or heterogeneous
107 reaction of nitrogen species such as HNO_3 , NO_3 , and N_2O_5 on the surface of dust and sea
108 salt aerosol particles (Bauer et al., 2004; 2005; Bian et al., 2003; Dentener 1996; Liao et
109 al., 2003), converts gas phase nitrogen species into aerosols. Consequently, the global
110 tropospheric NO_x concentration and the rate of conversion of N_2O_5 to HNO_3 will be
111 reduced (Riemer et al., 2003), which in turn leads to the reduction of atmospheric
112 oxidants. For example, global tropospheric O_3 can be reduced by 5% (Bauer et al., 2007)
113 and tropical Atlantic OH by 10% (Bian et al., 2003) just through the heterogeneous
114 reactions of nitrogen radicals on dust. Second, the most important removal path for
115 nitrogen from the atmosphere is the formation of HNO_3 , which is subsequently deposited
116 (Riemer et al., 2003). Since HNO_3 is subject to partitioning between the gas and aerosol
117 phases, the lifetimes of nitrogen species can be shortened by the formation of
118 tropospheric nitrate aerosol because the loss of total HNO_3 will be accelerated by a much
119 higher dry deposition in the aerosol phase.
120

121 Large nitrogen deposition occurs over both land and ocean (Dentener et al., 2006;
122 Kanakidou et al., 2012; 2016). Nitrogen deposition can either benefit or impair ecosystem
123 productivity depending on the initial balance of nutrients since different ecosystems have
124 different Nr (reactive nitrogen including gas and particulate NO_3^- and other nitrogen
125 compounds) availability and retention (Galloway et al., 2004; Prentice et al., 2001). If
126 fixed Nr is deposited as nitrate in forests, it may act as a "fertilizer," stimulating growth
127 and thus enhancing carbon sequestration (Fowler et al., 2015). But when the accumulated
128 deposition exceeds the nutritional needs of the ecosystem, nitrogen saturation may result
129 (Fenn et al., 1996). Soil fertility declines due to the leeching of cations (Milegroet and
130 Cole, 1984) and, thus, carbon uptake diminishes. The balance between fertilization and
131 saturation depends on the spatial and temporal extent of nitrogen deposition. In order to
132 determine the extent to which the emissions of air pollutants will have to be reduced and
133 whether the environment needs to be protected from damage, it is essential to know
134 where and by how much N deposition exceeds nature's tolerance (Dentener et al. 2006;
135 Lamarque et al., 2005; Phoenix et al., 2006).
136

137 Here we present a nitrate-focused study that has been organized as a part of the series of
138 AeroCom phase III experiments (<https://wiki.met.no/aerocom/phase3-experiments>). The
139 goals of this activity are to (1) address the diversity of the nitrate simulation by the
140 AeroCom multi-models and diagnose the driving processes for the diversity, (2) explore

141 the uncertainty of the model nitrate simulations constrained against various
142 measurements from ground station networks and aircraft campaigns, and (3) investigate
143 how the formation of nitrate changes in different models in response to perturbation on
144 key precursors and factors that determine nitrate formation. We focus on the first two
145 objectives in this paper. Such a study directs us on how to improve the representation of
146 nitrate aerosol formation and size distribution in climate chemistry models and reveals
147 nitrate effects on global air quality and climate.

148
149 Building upon the analysis of the multi-model diversity, three additional sensitivity
150 experiments are designed using the GMI model to further explore the potential sources
151 for the diversity on physical and chemical process-level. First, we explore the impact of
152 pH-dependent NH_3 wet deposition on atmospheric NH_3 and associated nitrogen species.
153 We then reveal the importance of mineral dust and sea salt in the nitrate formation and
154 check the resultant nitrate aerosol size distribution that is particularly important in nitrate
155 forcing estimation.

156
157 The paper is organized as follows. Section 2 introduces the experiment setup including
158 the emission inventories used and the participating AeroCom models. Observations of
159 surface tracer concentrations and dry and wet depositions over U.S., Europe, and East
160 Asia, as well as aircraft measurements in the ARCTAS campaigns are described in
161 section 3. We present AeroCom model inter-comparison and the model evaluation using
162 aforementioned observations in section 4. Based on the knowledge from previous
163 sections, we further discuss nitrate formation in response to physiochemical
164 methodologies in section 5 and summarize our major findings in section 6.

165 166 **2. Experiment setup and AeroCom model description**

167 168 **2.1 Experiment setup**

169 The AeroCom III nitrate experiment comprises one baseline and six perturbation
170 simulations, with the latter designed for assessing the possible future changes of emission
171 and meteorological fields relevant to nitrate formation. Models are advised to use the
172 same prescribed emission datasets for gases and aerosols. Emissions from anthropogenic,
173 aircraft, and ship for aerosol and ozone simulations are obtained from the recently
174 developed HTAP v2 database (Janssens-Maenhout et al., 2015) that provides high spatial
175 resolution monthly emission. For the tracers that are included in ozone chemistry but are
176 not provided by HTAP v2 (i.e. some volatile organic compounds), they should be
177 obtained from CMIP5 RCP85 with a linear interpolation between 2005 and 2010.
178 Biomass burning emissions are the emissions of GFED3 (Werf et al., 2010) in 2008
179 [<http://www.globalfiredata.org/data.html>]. The NH_3 emission from ocean is adopted
180 based on the compilation of GEIA emission inventory [Bouwman et al., 1997].
181 Participating modeling groups use their own emissions of dimethyl sulfide (DMS), dust,
182 sea salt, and NO from lightning, since they are calculated based on models'
183 meteorological fields.

184
185 A full year simulation for 2008 is required for the nitrate model experiment. There are
186 several in-situ observation datasets available in 2008 for model evaluation, including the

187 surface concentration and deposition measurements over the US (CastNet, AMoN,
188 NDAP/NTN), Europe (EMEP), and Asia (EANET), and the aircraft measurements of
189 vertical profiles (e.g. ARCTAS-A, ARCTAS-CARB, and ARCTAS-B). All participating
190 models are required to use the reanalysis or nudged meteorological data for 2008 and
191 allow one-year spin up for the baseline simulation.

192

193 **2.2 AeroCom models**

194 Nine models participate in the AeroCom III nitrate experiment. Their general nitrate-
195 related physiochemical mechanisms are summarized in Table 1. Further detailed
196 information on their thermodynamic equilibrium model (TEQM) is given in Table 2.

197

198 The models participating in this study are divided into two groups. Group one (CHASER,
199 EMAC, INCA, GISS-MATRIX, and GISS-OMA) run chemical fields together with
200 meteorological fields, while group two (EMEP, GMI, OsloCTM2, and OsloCTM3)
201 simulate chemical fields using archived meteorological fields. Most models in this study
202 have a horizontal resolution around 2-3 degrees except EMEP with 0.5 degree.

203 Vertically, most models cover both the troposphere and the stratosphere with a peak
204 altitude up to 0.01 hPa except EMEP that extends vertically up to 100 hPa into the
205 troposphere only.

206

207 All models use full gas phase O_3 - NO_x - HO_x chemistry to produce HNO_3 and consider the
208 feedback of nitrate aerosol formation on HNO_3 calculation ([i.e. changes in \$HNO_3\$](#)
209 [concentrations due to the gas/particle equilibrium](#)). [Meanwhile, all models consider \$N_2O_5\$](#)
210 [hydrolysis, the conversion of \$N_2O_5\$ to \$HNO_3\$. The first order loss reaction occurs on the](#)
211 [surface of tropospheric aerosols and assumes irreversible instant reaction. However, the](#)
212 [models differ in \$N_2O_5\$ hydrolysis by considering the reaction on the surface of different](#)
213 [aerosol types. Uptake coefficients \(aka gamma factors\) also differ in their relationship to](#)
214 [temperature and RH. CHASER model is special as it allows \$N_2O_5\$ conversion to \$HNO_3\$](#)
215 [on liquid cloud particles. Please refer to Table 1 and the listed references for details.](#)

216 [D](#)However, due to the complexity of chemical mechanisms for organic nitrate
217 compounds and different recommendations for reaction rates, HNO_3 fields produced by
218 the models differ greatly. This difference propagates into the subsequent gas-aerosol
219 reactions for nitrate formation.

220

221 These models are very different in their approaches on gas-aerosol reactions in nitrate
222 formation. All models consider reactions between NH_3 and HNO_3 . However, models
223 differ dramatically in whether to include [contributions of heterogeneous reactions on](#)-dust
224 [and sea salt](#)-(Table 1). Some account for both, some for only dust or sea salt, and some
225 do not account for any of them at all. The methods used by the models in accounting for
226 NH_3 and dust/sea salt contributions are also different. Please also note that the
227 heterogeneous chemical production of [particulate](#) nitrate mentioned in this paper refers
228 only to the [first order loss](#) reaction of HNO_3 on [the surface of](#) dust and sea salt particles.
229 A series of reactions, such as N_2O_5 hydrolysis and $BrONO_2$ hydrolysis, affect HNO_3
230 simulation. These reactions are typically considered in O_3 - NO_x - HO_x chemistry and their
231 discussion is beyond the scope of this paper.

232

233 All participating models adopt TEQM to deal with aqueous and solid phase reactions and
234 gas-aerosol partitioning (Tables 1 and 2). This is based on the assumption that volatile
235 species in the gas and aerosol phases are generally in chemical equilibrium. However, the
236 assumption is not always warranted in some cases, as we will discuss in section 5.2. Even
237 with the TEQM approach, nitrate calculation could differ due to treatments of
238 equilibrium constants or chemical potentials, solute activity coefficients, water activity,
239 and relative humidity of deliquescence (RHD). The parameterizations adopted by the
240 models to deal with multicomponent activity coefficient, binary activity coefficient, and
241 water activity are given in table 2. GISS-OMA, Oslo-CTM2 and Oslo-CTM3 are special
242 in that they assume aerosols to be metastable so that the model does not take into account
243 formation of solids in this study. All other models do consider the effect of the hysteresis
244 of particle phase transitions. All models also assume that the overall particles are large
245 enough to neglect the Kelvin effect.

246
247 The participating models call the TEQMs in different ways to account for aerosol size
248 effect. All the TEQMs (ISORROPIA-I, ISORROPIA-II, MARS, RPMIRES, INCA, and
249 EQSAM3) assume particles to be internally mixed, i.e. all particles of the same size have
250 the same composition. However, some parent models (CHASER, EMEP, GMI, INCA,
251 GISS-MATRIX and GISS-OMA) call their TEQMs only once for fine mode aerosol
252 particles, while the others (EMAC, OsloCTM2 and OsloCTM3) call their TEQMs from
253 different aerosol size bins. For example, Oslo-CTM2 and Oslo-CTM3 consider a bi-
254 modal aerosol size-spectrum with two major aerosol modes, fine and coarse, and
255 calculate gas-aerosol equilibrium partitioning with EQSAM3 first for fine mode and then
256 for coarse mode. Additionally, to account for kinetic limitations, EMAC calculates the
257 phase partitioning in two stages. In the first stage, the amount of the gas-phase species
258 that is able to kinetically condense onto the aerosol phase within the model time step is
259 calculated, while in the second stage, the TEQM redistributes the mass between the two
260 phases assuming instant equilibrium (Pringle et al., 2010).

261
262 The TEQMs also differ in the chemical components considered. Specifically, the TEQMs
263 in CHASE, EMEP, GISS-MATRIX, GISS-OMA, GMI and INCA include only species
264 of sulfate, nitrate, ammonium and their gas, liquid, and solid components. The models
265 Oslo-CTM2 and Oslo-CTM3 add NaCl and HCl, while the model EMAC further expands
266 the species by including dust-related crustal material such as Ca^{2+} , K^+ , and Mg^{2+} .

267
268 These TEQMs differ in their computational approaches as well. Computational efficiency
269 is a prime consideration for a TEQM that is designed for incorporation into a global air
270 quality and climate study. To speed up the calculation, TEQMs typically divide the
271 system into sub-domains based on RH and concentrations of ammonium, sodium, crustal
272 cations, and sulfate. Corresponding approximation could be adopted for each sub-domain
273 with the minimum numbers of equilibriums and unknown components. As listed in table
274 2, the numbers of sub-domains are 4, 5, 4, 2, 3, and 3 for the TEQM ISORROPIA-I,
275 ISORROPIA-II, MARS, RPMIRES, INCA, and EQSAM3, respectively.

276
277 The ways to account for the contribution of dust and sea salt to nitrate formation are also
278 different ([see Table 1 column "How do CHEMDUSS"](#)). Some models (EMAC, Oslo-

279 CTM3, and Oslo-CTM2) include dust and/or sea salt components in their TEQM models
280 directly ([marked as TEQM in Table 1 under column “How do CHEMDUSS”](#)), while
281 some models (EMEP, GISS-OMA, GMI, and INCA) use an approach of first order loss
282 rate outside their TEQMs to account for the heterogeneous reactions of HNO₃ on the
283 surface of dust and sea salt ([marked as HETCHEM in Table 1](#)). For the latter approach,
284 the gamma rates and their RH dependence adopted by the models differ as well.

Formatted: Subscript

285
286 Dry and wet deposition of NH₃, ammonium nitrate, and ammonium sulfate are treated
287 similarly to other gas and aerosol tracers in the models. It is worth pointing out that there
288 is a different consideration for Henry’s law constant of NH₃ used by the models. Some
289 models modify it based on the pH value of cloud water while others do not. We will
290 discuss the impact of these two treatments on nitrate simulation in section 5.1.

291
292 We introduce only the major characteristics of thermodynamic equilibrium models since
293 this study aims for the evaluation and explanation of overall nitrate diversity among the
294 GCM/CTM models from all potential aspects. The detailed discussion of the models
295 chemical mechanism of gas phase reactions and the aerosol optical properties adopted by
296 the models is also beyond this work. Readers could refer to the references listed in Tables
297 1 and 2 for any further details.

298 299 **3. Observations**

300 We use surface measurements from ground station networks and aircraft campaigns to
301 evaluate modeled surface concentrations, dry and wet depositions, and vertical
302 distributions of nitrate and related species (Table 3).

303 304 **3.1 Surface measurements of concentrations and deposition rates**

305 Ambient concentrations of sulfur and nitrogen species throughout the US and Canada
306 have been measured by the ground station network CASTNET (Clean Air Status and
307 Trends Network) (Figure 1). The measurements use a 3-stage filter pack with a controlled
308 flow rate. The measurements of CASTNET do not include NH₃. AMoN (Ammonia
309 Monitoring Network), measuring concentrations of ambient NH₃, has been deployed at
310 CASTNET sites starting from October 2007 using passive samplers. The corresponding
311 tracers’ surface concentration measurements over Europe have been conducted by EMEP
312 (The European Monitoring and Evaluation Programme). The measured sites of all these
313 networks are located in rural areas or sensitive ecosystems, representing a larger region
314 by avoiding influences and contamination from local sources. Surface concentrations
315 over East Asia are inferred from the measurement of dry deposition by EANET (Acid
316 Deposition Monitoring Network in East Asia). This network provides acid deposition
317 from a regional monitoring network including 13 countries in East Asia using
318 standardized monitoring methods and analytical techniques.

319
320 CASTNET also provides dry deposition of sulfate and nitrogen species. Direct
321 measurements of dry deposition fluxes (D) are expensive so D is calculated as the
322 measured pollutant concentration (C) multiplied by the modeled dry deposition velocity
323 (V_d). V_d is either estimated by the Multi-Layer Model fed with measured hourly

324 meteorological data or derived from historical average V_d for sites with discontinued
325 meteorological parameters.

326

327 Direct measurements of wet deposition fluxes of sulfate, nitrate, and other ions have also
328 been performed by NADP/NTN (the National Atmospheric Deposition Program /
329 National Trends Network) across the contiguous US, Canada, Alaska, and the US Virgin
330 Islands and EANET over East Asia. Sites are predominantly located away from urban
331 areas and point sources of pollution. Each site has a precipitation chemistry collector and
332 gauge. Both networks can measure wet deposition for a continuous period (weekly for
333 NADP/NTN and daily for EANET), or every precipitation event if using an automated
334 collector (wet-only sampling).

335

336 Data is quality assured for all measurements. Measurements over North America use
337 automated screening techniques, semi-annual calibration results, site operator comments,
338 and manual data review. Quality assurance of EMEP is carried out on both the national
339 level and by the Chemical Co-ordinating Centre (CCC). The quality of EMEP
340 measurements is not equal at the national level (Schaap et al., 2002; 2004). Sites in
341 North, Western and Central Europe were generally well equipped and performing, while
342 sites in the rest of Europe suffered from inadequate sampling and calibrating methods due
343 to political and/or economical reasons. The quality of ammonia measurement is relatively
344 low since some laboratories experienced contamination problems (Williams et al., 1992).
345 Although EANET adopts standardized monitoring methods and analytical techniques,
346 quality assurance is carried out on the national level.

347

348 **3.2 Aircraft measurements of vertical profiles**

349 Aircraft campaign measurements during the 2008 Arctic Research of the Composition of
350 the Troposphere from Aircraft and Satellites (ARCTAS) are used to evaluate tracer
351 vertical distribution simulated by the models (Bian et al., 2013; Jacob et al., 2010). Three
352 phases of the campaign, ranging from Northern Hemisphere mid-latitude industrial
353 region (ARCTAS-CARB, June 2008) to high latitude Arctic regions influenced by long-
354 rang pollution transport (ARCTAS-A, April 2008) and by local boreal biomass burning
355 (ARCTAS-B, July 2008), provide well encompassing environment observations. All
356 flights were conducted by the NASA DC-8 aircraft and the flight tracks of these three
357 phases are presented in Figure 2. An onboard HR-ToF-AMS instrument (Cubison et al.,
358 2011; DeCarlo et al., 2006) measured fine mode aerosol concentrations (PM₁) along the
359 flight track including NO_3^- , NH_4^+ , and SO_4^{2-} at STP conditions (1013mb and 273.15K) at a
360 sampling time interval of ~12 seconds. Accuracy estimate of 2-standard deviations, likely
361 conservative, is 34% for inorganics, dominated by the uncertainty in particle collection
362 efficiency due to particle bouncing (Huffman et al., 2005).

363

364 **4. Model intercomparison and evaluation**

365

366 **4.1 AeroCom model inter-comparisons of global distributions and budgets**

367 **4.1.1 NH_3 and NH_4^+**

368 Six models use HTAP2 anthropogenic emissions, two (GISS-MATRIX and GISS-OMA)
369 use CMIP5 emissions, and one (INCA) uses ECLIPSE emissions. Table 4b shows that

370 eight models have the annual NH_3 emission values within 5% of the value from the
371 AeroCom experiment recommended emission inventories, but INCA is 11% higher. The
372 similar emission distributions ensure that the examined inter-model diversities are truly
373 caused by the differences in physicochemical processes among the models. The
374 normalized root-mean-square deviation (NRMSD) of NH_3 global burden among models
375 is 1.17 and 0.33 with and without EMAC included. This drastic change in global burden
376 NRMSD by EMAC is caused by its special treatment of wet deposition. In fact, the
377 removal of trace gases and aerosol particles by clouds and precipitation in EMAC is not
378 calculated based on empirically determined, fixed scavenging coefficients, but rather by
379 solving a system of coupled ordinary differential equations, explicitly describing the
380 processes involved (Tost et al., 2006). This method resolves feedback mechanisms
381 between the multi-phase chemistry and transport processes involved. The liquid phase
382 reaction set used converts all the scavenged NH_3 (or HNO_3) into NH_4^+ (or NO_3^-) in the
383 liquid phase so that at the end everything that is deposited is the total NH_4^+ and NH_3 .

384
385 Atmospheric NH_4^+ is produced entirely by NH_3 chemical transformation. The models
386 simulate NH_4^+ much closer in chemical production (difference less than a factor of 2) than
387 in lifetime (difference up to a factor of 5.2), indicating removing rates are a key factor in
388 controlling the global burden of NH_4^+ . For example, CHASER has a much longer lifetime
389 of NH_4^+ (i.e. 9.8 days versus 4.3 days in average), which indicates a slow deposition
390 removal of NH_4^+ from the atmosphere. Consequently, CHASER simulates a much higher
391 atmospheric NH_4^+ burden than other models.

392

393 4.1.2 HNO_3 and NO_3^-

394 HNO_3 , an important nitrate precursor, differs by up to a factor of 9 in its global
395 tropospheric burden among the models (Table 4c). All models simulated HNO_3 based on
396 a full gas phase O_3 - HO_x - NO_x chemistry and coupled it with aerosol chemistry. This
397 HNO_3 diversity will naturally be propagated into the NO_3^- simulation. However, further
398 discussion of the detailed consideration of full gas-aerosol chemistry for HNO_3 diversity
399 among the models is beyond the scope of this study.

400

401 The resultant aerosol product (i.e., NO_3^-) does not entirely follow its precursor (i.e.,
402 HNO_3) in terms of global burden: EMEP has very low HNO_3 but high NO_3^- , two GISS
403 models (MATRIX and OMA) simulate high HNO_3 but low NO_3^- , while OsloCTM3 has
404 an average HNO_3 but more than triple high NO_3^- than average (Tables 4a and 4c).
405 Furthermore, the difference in NO_3^- global burden (up to a factor of 13) is larger than that
406 of HNO_3 . Differences in chemical mechanisms of NO_3^- production could be a potential
407 explanation along with the difference in HNO_3 precursor. Unfortunately, only GMI and
408 INCA provide a detailed NO_3^- chemistry budget analysis. Nevertheless, we can infer that
409 the total chemical production of NO_3^- must be very low ($\sim 10\text{Tg}$) in the two GISS models
410 while very high ($> 100\text{Tg}$) in OsloCTM2 and OsloCTM3 based on the reported total
411 NO_3^- loss. Combining this information with the HNO_3 global tropospheric burden (Table
412 4c), we can further infer that the chemical conversion from HNO_3 to NO_3^- must be lowest
413 in the two GISS models while highest in the two Oslo models. Several factors could
414 influence this conversion, such as the availability of alkaline species of mineral dust and
415 sea-salt particles and the physicochemical mechanism of nitrate formation on dust and

416 sea-salt, availability of NH_3 after combining with SO_4^{2-} , and the atmospheric
417 meteorological fields of temperature and relative humidity. More discussions are given in
418 sections 5.2 and 5.3.

419

420 Atmospheric lifetime of NO_3^- differs up to a factor of 4, from about 2 days in GMI and
421 OsloCTM2 to larger than 7 days in GISS-OMA and GISS-MATRIX. The slower removal
422 processes in the two GISS models compensate the low chemical production and help to
423 maintain their NO_3^- atmospheric burden (Figure 3 and Table 4a).

424

425 **4.2 Model-observation comparisons**

426

427 **4.2.1 Comparisons of surface concentrations over North America, Europe, and East** 428 **Asia**

429 Understanding diversity among model simulations and potential physiochemical
430 processes behind the difference is important but not sufficient. The information has to be
431 combined with the knowledge of model performance obtained directly from comparisons,
432 particularly down to processes level, against various measurements to gain a direction of
433 any improvement. Figures 4a-c show a model-observation comparison for surface
434 mass/volume mixing ratios of NO_3^- , NH_4^+ , NH_3 , HNO_3 , and SO_4^{2-} over North America
435 (CastNET), Europe (EMEP), and East Asia (EANET). Each point represents a monthly
436 mean concentration at one observational site. Generally, the agreement between model
437 and observation is better for aerosol components than for gas tracers (i.e. the precursor
438 species NH_3 and HNO_3) over all three regions. All models underestimate NH_3 surface
439 volume mixing ratio with a ratio of model to observation down to 0.14, while most
440 models overestimate surface HNO_3 volume mixing ratio with a ratio up to 3.9 over North
441 America. The worse performances of NH_3 against observations may be also associated to
442 their relatively lower measurement accuracy, i.e. easier to be contaminated during
443 measurement (Williams et al., 1992). Among aerosol simulations, model performance is
444 very similar for NH_4^+ and SO_4^{2-} , while slightly worse for NO_3^- that is dispersed further
445 away from the 1:1 line, particularly at low NO_3^- values. The NO_3^- simulation over East
446 Asia is worst with the average normalized root mean square to be 1.3 and 1.8 higher than
447 that over North America and Europe, respectively.

448

449 **4.2.2 Comparisons of vertical profiles with aircraft measurements during the** 450 **ARCTAS field campaign**

451 Evaluation of model performance presented in 4.2.1 for the surface concentrations in the
452 source regions is highly dependent on the accuracy of the emission inventory. On the
453 other hand, evaluation using aircraft measurements, particularly over remote regions,
454 provides further examination of models' physicochemical evolution during transport.
455 Here we use data from three phases of the ARCTAS aircraft campaign (section 3), and
456 the results are shown in Figure 5. All model results of NO_3^- , NH_4^+ , and SO_4^{2-} are sampled
457 along flight track and averaged regionally within 1km vertically for each campaign phase
458 before comparing with the corresponding aircraft measurements. Note that only EMAC,
459 EMEP and GMI report daily 3D global tracer concentrations, while the others report
460 monthly only. Note also that only EMEP and GMI adopt daily biomass burning emission
461 while the others use monthly emission. To verify the representativeness of monthly mean

462 concentration in capturing the main features exhibited in model-observation comparisons,
463 daily and monthly concentrations of the three models are used in the same spatial
464 sampling to compare with the measurements (see the green lines for daily and red for
465 monthly in the figure). The comparison keeps its main features as shown when using both
466 daily and monthly model data.

467

468 During ARCTAS-A, which was conducted in April 2008 and was based in Fairbanks,
469 Alaska, none of the models captures the long-range transport of aerosols primarily from
470 Asia, which enter Polar Regions at altitudes between 2-7 km (Fig. 3 in Bian et al., 2013).
471 Except CHASER and EMAC, all models also report a significant underestimation of
472 NH_4^+ and SO_4^{2-} in boundary layer. A previous assessment of pollution transport to the
473 Arctic indicated that aerosol wet removal plays an important role in the uncertainty of
474 Arctic aerosols (Shindell et al., 2008). Another potential reason is that some large fire
475 activities in Siberia during April 2008 (Jacob et al., 2010) may be missed in the GFED3
476 emission inventory. The underestimation of SO_4^{2-} may help bring up NO_3^- production,
477 particularly at high altitudes. During ARCTAS-CARB, which was conducted in June
478 2008 based in Palmdale, California, agreement between model and measurements is
479 much improved. Almost all models show a rapid vertical decrease from surface to free
480 troposphere, which is consistent with the measurements of SO_4^{2-} and NH_4^+ , but not NO_3^- .
481 The observation shows a maximum of NO_3^- at about 1.5 km, which is not represented by
482 any of the models. During ARCTAS-B, which was conducted in July 2008 and was based
483 in Cold Lake, Canada, when there were frequent local wild fires, model performances are
484 mixed. In general, most models underestimate concentrations of NO_3^- , NH_4^+ and
485 SO_4^{2-} below 4 km. CHASER model is special in that it overestimates SO_4^{2-} significantly.
486 This may be contributed to high (near surface) to comparable (free troposphere) model
487 simulation of NH_4^+ but an underestimation of NO_3^- . Different from other models, the
488 INCA model shows an enhancement of pollutants in the upper troposphere with
489 concentrations much higher (more than 5 times) than observations. This behavior may be
490 derived from a much vigorous vertical uplifting to the upper troposphere as revealed from
491 Fig. 3a-3b combined with a low NH_3 Henry's law constant used by INCA, see discussion
492 in section 5.2.

493

494 Note that all measurements and model data we discussed above are for fine mode
495 aerosols. Total NO_3^- (orange line using monthly model output) is also shown in the figure
496 to reveal whether a changing of partitioning of fine and coarse mode NO_3^- could improve
497 the model-observation comparison. It seems that the new version of OsloCTM3 may put
498 too much of NO_3^- in coarse mode.

499

500 **4.3 Model-observation comparison for dry and wet deposition**

501

502 **4.3.1 Dry deposition**

503 The budget analyses in section 4.1 concluded that dry and/or wet depositions are most
504 likely the main processes driving the diversity in the model simulations. Thus, further
505 evaluation of deposition processes is needed to identify any potential problematic model.

506

507 The dry depositions of NO_3^- , NH_4^+ , HNO_3 , and SO_4^{2-} simulated by the models are
508 compared against CASTNET measurements over North America (Figure 6). Generally,
509 the overestimation of surface HNO_3 concentrations (Figure 3a) results in the higher dry
510 depositions of HNO_3 , but this is not the case for NO_3^- . Meanwhile, most of the models
511 give a better dry deposition simulation for aerosol SO_4^{2-} and NH_4^+ than for aerosol NO_3^- ,
512 except CHASER. Specifically, GISS-OMA and GISS-MATRIX have wide spread dry
513 NO_3^- deposition at any given measurement value. In other words, the two models
514 underestimate NO_3^- dry deposition significantly at many observational stations, which
515 does not occur in the other models. This low dry deposition simulation may occur outside
516 North America as well because the global dry depositions of the two models are lower
517 than others (Table 4a). OsloCTM2 overestimates NO_3^- dry deposition significantly, which
518 is probably linked to its larger coarse fraction of the nitrate aerosol (see discussion in
519 section 5.3). OsloCTM3 improved its dry deposition scheme although the model still
520 overestimates the dry deposition. We will discuss the OsloCTM2 NO_3^- simulation over
521 North America by combining the model's wet deposition in the next section. NH_4^+ dry
522 deposition is low in GMI but very high in CHASER. This performance is also extended
523 globally as summarized in Table 4b.

524

525 **4.3.2 Wet deposition**

526 The wet deposition simulations from the nine models are compared with surface
527 measurement over North America (Figure 7a) and East Asia (Figure 7b) for oxidized
528 NO_3^- (i.e. total NO_3^- and HNO_3), total NH_4^+ and NH_3 (tNH_4^+), and SO_4^{2-} . All models tend
529 to underestimate the wet deposition of tNH_4^+ and SO_4^{2-} over the two regions. Models
530 EMAC, GMI, OsloCTM2 and OsloCTM3 have relatively high wet removal for oxidized
531 NO_3^- , while EMEP removes much less than others over North America. All models' wet
532 deposition of oxidized NO_3^- is biased low over East Asia. As we discussed above,
533 OsloCTM2 and OsloCTM3 have very high dry NO_3^- depositions (Figure 6) compared
534 with CASTNET observations. The overall high dry and wet NO_3^- depositions along with
535 high atmospheric concentrations (Figure 4a) indicate that the chemical formation of
536 NO_3^- in the two models must be also high. This performance might be also true on global
537 scale since the inferred chemical productions of NO_3^- in the two models are the highest
538 (Table 4a). CHASER has the lowest tNH_4^+ wet deposition. This may result in a very high
539 NH_4^+ dry deposition (Figure 6) and concentration (Figures 4a-c, 5) compared with
540 observations and other models. Overall, wet deposition seems to be the dominant process
541 in determining the diversity in NH_3 and NH_4^+ lifetime (Table 4b).

542

543 Note that we use the traditional approach of comparing models' grid box mean values
544 with observations, which does not take into account the impact of the models' horizontal
545 resolutions in their representation of observations (Schutgens et al., 2016). Since majority
546 models (except EMEP) have horizontal resolutions around 2-3 degrees, the models grid
547 box means tend to smooth out extreme (i.e. very low or high) observations.
548 Consequently, the slopes of the fitting lines are generally less than 1 on the scattering
549 plots with model as y-axis and observation as x-axis (e.g. Figures 4a-d, 6, 7a-b).

550

551 **5. Discussion of major uncertainties in nitrate formation**

552 Large uncertainties of nitrate studies result from the complexity of the simulations which

553 must consider a comprehensive NO_x-NMHC-O₃-NH₃ chemistry and a thermodynamic
 554 equilibrium model (TEQM) to partition semi-volatile ammonium nitrate between the gas
 555 and aerosol phases. Nitrate aerosol concentrations depend on temperature, relative
 556 humidity (RH), and concentrations of HNO₃, NH₃, NH₄⁺, SO₄²⁻, Cl⁻, Na⁺, Ca²⁺, K⁺,
 557 Mg²⁺, organic acids, among others. A further complicating factor is that the equilibrium
 558 for the coarse mode is somewhat questionable (Feng and Penner, 2007). In addition, wet
 559 removal of NH₃ is very sensitive to the pH in cloud water. We will discuss some of these
 560 uncertainties below.

561

562 **5.1 pH-dependent NH₃ wet deposition**

563 Gas tracer NH₃, a precursor of ammonium aerosol, experiences atmospheric wet
 564 deposition and its deposition rate is typically calculated using Henry's Law. Henry's law
 565 constant (H) of gases in water is usually given at 298 K (indicated by Θ in superscript)
 566 and can be adjusted by temperature (T).

$$H(T) = H^{\Theta} * \exp\left(-\frac{\Delta H_{sol}}{R}\left(\frac{1}{T} - \frac{1}{T^{\Theta}}\right)\right) \quad (1)$$

567 Here ΔH_{sol} is the enthalpy of dissolution and R is the gas constant.

568

569 For some acidic/basic gases, including NH₃, Henry's law constant is also a function of
 570 pH in cloud water (a.k.a effective Henry's law constant H^{Θ*}). As explained in the
 571 Appendix, the H^{Θ*} is inferred from H^Θ with a correction of pH (pH = -log₁₀[H⁺]) as

$$H^{\Theta*} = H^{\Theta} \frac{K_{al}[H^+]}{K_w} \quad (5)$$

572 Here, K_{al} ≈ 1.8x10⁻⁵ and K_w = 1.0x10⁻¹⁴ at 298 K in pure water (see Appendix). However,
 573 not every model accounts for pH adjustment (i.e. the reaction of equation 2 in Appendix)
 574 for NH₃ dissolution. More accurately, the EMAC model implicitly calculates the
 575 effective Henry's law constant by solving a set of partial differential equations, which
 576 includes not only the gas-liquid phase equilibria, but also the reactions in the liquid phase
 577 (i.e. dissociation or acid-base equilibria, Redox reactions and photolysis reactions in the
 578 liquid phase, see Tost et al.(2006)). Therefore, the gas-liquid phase equilibrium is
 579 explicitly calculated based on the chemical mechanism used in the liquid phase. As listed
 580 in Table 5, the rest of the models are generally divided into two groups based on their
 581 effective Henry's law constant: (1) INCA, GISS-OMA and GISS-MATRIX has H^{Θ*} ≤
 582 100 (L-theta without pH correction) and (2) CHASER, GMI, OsloCTM2 and Oslo-
 583 CTM3 has H^{Θ*} > 10⁺⁵ (H-theta with pH correction). The NH₃'s H^{Θ*} adopted by the
 584 models varies dramatically, up to an order of 6 in magnitude among all the models and a
 585 factor of 10 just for the models in H-theta group (Table 5). The latter corresponds to a
 586 range of pH from 4.5 (Oslo-CTM2) to 5.5 (CHASER).

587

588 To examine how sensitive of NH₃, NH₄⁺ and NO₃⁻ simulations in response to the
 589 magnitude of NH₃'s H^{Θ*}, we performed a sensitivity experiment, named TWET, in the
 590 GMI model in which there was no pH adjustment for NH₃ Henry's law constant (i.e.
 591 H^{Θ*}=61 instead of 1.05e+6, see table 6). The resultant annual budgets of dry/wet
 592 deposition, chemistry production and loss, and atmospheric loading of NH₃,
 593 NH₄⁺ and NO₃⁻ are summarized in Table 7, the tracers' vertical zonal mean distributions
 594 are shown in Figure 8, and the comparisons with the ARCTAS measurements for

595 NH_4^+ and NO_3^- are shown in Figure 9. For convenient comparison, the GMI baseline
596 results are given in the table and figures as well. There is a dramatic decrease (from 17.5
597 to 1.1 Tg) in NH_3 wet deposition when using pure water NH_3 Henry's law constant.
598 Consequently, NH_3 will remain in the atmosphere (i.e. ~ 8 times more atmospheric NH_3)
599 to produce ~1.6 times more NH_4^+ chemically. This, in turn, greatly increases atmospheric
600 NO_3^- to 0.97 Tg from 0.26 Tg reported in baseline simulation. A large portion of the
601 increased NH_3 , NH_4^+ and NO_3^- resides in the upper troposphere and close to the
602 tropopause region, while the changes of the tracers in the lower troposphere are relatively
603 small, as shown in Figure 8. These accumulations at high altitudes are far above (i.e. ~ 50
604 times for NH_4^+ and NO_3^-) the ARCTAS observed tracer amounts as shown in Figure 9.
605 The TWET experiment might be an explanation of NH_4^+ and NO_3^- accumulations near the
606 tropopause region (Figure 3a-b) in the INCA model whose NH_3 Henry's law constant H^\ominus
607 is 74 without pH correction (i.e. a L-theta model, table 5). However, it is puzzling that the
608 NH_3 simulations by GISS-MATRIX and GISS-OMA, those are the models with L-theta,
609 are closer to the simulations of the models with H-theta, i.e. no NH_4^+ and NO_3^-
610 accumulation near the tropopause and comparable removal of NH_4^+ (Figure 3a-b and
611 Table 4b).

612

613 **5.2 Contribution of dust and sea salt on nitrate formation**

614 In the presence of acidic accumulation-mode sulfuric acid containing aerosols, HNO_3 ,
615 NO_3 radicals, and N_2O_5 will deposit on larger alkaline mineral or salt particles (Dentener
616 et al., 1996; Gard et al., 1998; Hauglustaine 2014; Karydis et al., 2016; Murphy and
617 Thomson 1997; Paulot et al., 2016). Considerable evidence shows that the majority of
618 atmospheric nitrate is formed via reactions associated with dust and sea salt (Allen et al.
619 2015; Itahashi et al., 2016; Karydis et al., 2016). Coarse mode nitrate overwhelmingly
620 dominates over remote oceanic regions (Itahashi et al., 2016). Over wide land regions,
621 nitrate also quite often exists in the form of supermicron NO_3^- balanced by the presence
622 of mineral cations arising from transport of crustal dust and sea spray aerosol (Allen et
623 al.,2015; Lefer and Talbot; 2001).

624

625 Investigation of nitrate interactions with mineral dust and sea salt depends on the
626 simulation approach adopted in a model. The traditional equilibrium approach to partition
627 semi-volatile HNO_3 between the gas and aerosol phases is no longer possible since the
628 time to reach equilibrium on coarse mode particles (several hours to days) is typically
629 much longer than the chemical time step used in a global model (less than 1 hour) (John
630 et al., 1989; Myhre et al., 2006). Meng and Seinfeld (1996) found that on longer time
631 scales, when NH_3/HNO_3 started to condense on larger aerosols, their gas phase
632 concentrations decreased so that some of the condensed matter can be driven back to the
633 gas phase from the small semi-volatile aerosols. A fix to a non-equilibrium state would
634 be to implement a kinetic formulation for the particles that have a long equilibrium time
635 scale (Feng and Penner, 2007; Karydis et al., 2010). However, implementing explicit
636 kinetics in a global model would be computationally expensive and, hence, is not feasible
637 for long-term climate simulations. Several approximations have been developed to allow
638 computational efficiency although they might compromise model accuracy~~Several~~
639 ~~approximations, therefore, have been developed to compromise accuracy and efficiency.~~
640

641 Four such approximations are adopted by the nine models participating in this study: 1)
642 using equilibrium calculations for fine mode particles only while neglecting nitrate
643 formation on coarse mode particles (CHASER and GISS-MATRIX); 2) combining
644 equilibrium calculation for a solution of SO_4^{2-} - NO_3^- - NH_4^+ - H_2O and heterogeneous
645 reaction calculation for nitrogen uptake on dust and sea-salt using a first-order loss rate
646 (EMEP, GMI, GISS-OMA and INCA); 3) running equilibrium model including NH_3 ,
647 dust and sea salt repeatedly for aerosol sizes from fine mode to coarse mode (Oslo-CTM2
648 and Oslo-CTM3); and 4) using only the fraction of the gas that can kinetically condense
649 within the time step of the model in the equilibrium calculations for each aerosol size
650 mode (EMAC).

651
652 Nitrate is formed primarily on dust and sea salt by GMI (88%) and INCA (82%) (see
653 Table 4a). INCA further separates the formation as 45% on dust and 37% on sea-salt. The
654 above-mentioned approach 1 is problematic due to absence of coarse mode nitrate, an
655 important portion of nitrate, which results in relatively low nitrate burdens for CHASER
656 and GISS-MATRIX. Unfortunately, the other models are missing a detailed nitrate
657 chemistry budget report. A potential impact of dust and sea-salt on nitrate formation,
658 nevertheless, can be inferred from the approach adopted by a model. For example,
659 OsloCTM2 and OsloCTM3 adopt approach 3. Although the model allows fine mode
660 particles to reach equilibrium first, the subsequent equilibrium calculation for coarse
661 mode particles may still produce coarse mode nitrate too quickly, see discussion of the
662 ratio of coarse model nitrate in the next subsection. To avoid such overestimations on the
663 production of coarse mode nitrate, EMAC allows only a fraction of HNO_3 to partition in
664 the aerosol phase by assuming diffusion limited condensation (Pringle et al., 2010).

665
666 To further understand the role of homogeneous and heterogeneous chemical reaction
667 processes in nitrate formation, we conducted two more sensitivity experiments,
668 TnoCNH3 and TnoCHET, with the GMI model (Table 6). Experiment TnoCNH3 turned
669 off chemical conversion of NH_3 to NH_4^+ in the GMI thermodynamic equilibrium model,
670 while experiment TnoCHET excluded the nitrate formation via heterogeneous reaction of
671 gas HNO_3 on the particles of dust and sea salt. The budget report, vertical zonal mean
672 distribution and model-observation comparison of NH_3 , NH_4^+ and NO_3^- are given in Table
673 7 and Figures 8-9, respectively. It is not surprising that experiment TnoCNH3 gives a
674 higher atmospheric NH_3 burden (0.32 Tg) compared with baseline (0.11 Tg) with little
675 NH_4^+ left (from its initial field). The interesting thing is that the formed NO_3^- has only
676 slightly decreased compared with baseline (from 0.26 to 0.20 Tg), confirming the
677 importance of NO_3^- formation via dust and sea salt. For experiment TnoCHET, the
678 simulations of NH_3 and NH_4^+ stay the same but the formed NO_3^- is decreased dramatically
679 (from 0.26 to 0.10), indicating that NO_3^- formation via NH_3 chemistry alone in the GMI
680 model is relatively small. The chemical production of NO_3^- is about 6 times larger in
681 TnoCNH3 (via dust and sea salt) than in TnoCHET (via NH_3). However, the NO_3^-
682 produced via NH_3 chemistry (TnoCHET) is non-negligible over remote regions impacted
683 by long-range transport, as shown in the analysis of April Alaska observations in Figure
684 9.

685
686 **5.3 Nitrate size distribution**

687 Unlike sulfate aerosol, a noticeable fraction of nitrate aerosol is in coarse mode. Coarse
688 mode aerosol nitrate is formed due to presence of dust and/or sea salt. In other words, the
689 formation of nitrate on coarse mode dust and sea salt particles is the major factor
690 controlling size distribution. Other factors, such as $\text{NH}_3/\text{NH}_4^+/\text{NO}_3^-$ chemistry and
691 atmospheric transport and removal processes, also affect nitrate size distribution. Having
692 an accurate aerosol size distribution is critical in climate forcing estimations, since large
693 size particles have a relatively small optical cross section at a given aerosol mass loading
694 and the nitrate material coating on dust particles has almost no direct impact on the dust
695 optics, although the greatly impact dust lifetime (Bauer et al., 2007). Given that the
696 deposition velocity of a coarse particle is greater than that of a fine particle, an accurate
697 size distribution is also necessary to estimate deposition of particulate nitrates (Yeatman
698 et al., 2001; Sadanaga et al., 2008). This estimation is particularly important over oceans
699 where coarse mode nitrate dominates (Itahashi et al., 2016) and nitrogen supply is often
700 in deficit (Hansell and Follows, 2008).

701
702 As we have discussed in section 5.2, nitrate size distribution varies with the approaches
703 adopted for nitrate formation on coarse mode aerosols (i.e. dust and sea salt). Figure 10
704 gives the burdens of nitrate in fine mode and coarse mode portions and the ratio between
705 coarse mode and total (f_c) for the eight discussed models. The ratio is ranging from 0
706 (CHASER and GISS-OMA), ~50% (EMAC, GMI and INCA), ~80% (EMEP and
707 OsloCTM2), and 97% (OsloCTM3). The two OsloCTMs give the highest f_c partially
708 because they run TEQM model for coarse model particles.

709
710 A wide range of f_c , from 0 to > 90%, has been reported previously by model simulations
711 (Adams et al., 2001; Bauer et al., 2007; Jacobson 2001), while the range is narrowed
712 down to 40-60% for the model studies using the approach that solves dynamic mass
713 transfer equation for coarse mode particles (Feng and Penner, 2007; Xu and Penner,
714 2012).

715
716 It is worth pointing out that aerosol microphysics modify aerosol size as well. For
717 example, a process like coagulation would also allow NO_3^- to mix with other particles and
718 enter coarse mode aerosol. New particle formation/nucleation would add $\text{NH}_3/\text{NH}_4^+/\text{NO}_3^-$
719 into the ultra fine mode. Except EMAC and GISS-MATRIX, majority models involved in
720 this study are bulk aerosol models that do not account for aerosol microphysics.

721
722 It is challenging to verify the nitrate size distribution globally due to the limited
723 measurements on time and space. Measurements over regional and station sites indicated
724 that the ratio of f_c could be very high and vary seasonally over oceanic sites. For
725 example, annual mean f_c during 2002-2004 from the Fukue supersite observatory is
726 about 72% with a seasonal variation of 60–80% in winter and of around 80% in summer
727 (Itahashi et al., 2016).

728
729 However, the ratio could be varied dramatically over land or the areas affected by land
730 pollution. For example, observations of fine and coarse particulate nitrate at several rural
731 locations in the United States indicated that nitrate was predominantly in submicron
732 ammonium nitrate particles during the Bondville and San Gorgonio (April) campaigns, in

733 coarse mode nitrate particles at Grand Canyon (May) and Great Smoky Mountains
734 (July/August), and both fine and coarse mode nitrate during the studies at Brigantine and
735 San Gorgonio (July) (Lee et al., 2008). Allen et al. (2015) examined aerosol composition
736 data collected during the summer 2013 SOAS and concluded that inorganic nitrate in the
737 southeastern United States likely exists in the form of supermicron NO_3^- , balanced by the
738 presence of mineral cations arising from the transport of crustal dust and sea spray
739 aerosol. The measurements over Harvard Forest, a rural site in central Massachusetts,
740 supported that the majority of nitrate mass was associated with water-soluble
741 supermicron soil-derived Ca^{2+} in an acidic environment (Lefer and Talbot, 2001).
742 [Measurements taken in Paris during the ESQUIF campaign found that the coarse](#)
743 [nitrate fraction represents up to 60% of total particulate nitrate mass at night and 80% at](#)
744 [day \(Hodzic et al., 2006a, 2006b\)](#). Measurements of coarse-mode aerosol nitrate and
745 ammonium at two polluted coastal sites, Weybourne, England and Mace Head, Ireland,
746 during polluted flow when the air had passed over strong source regions of the UK and
747 northern Europe, showed 40–60% of the nitrate was found in particles with diameter
748 $>1 \mu\text{m}$, but under clean marine conditions almost 100% conversion was seen (Yeatman et
749 al., 2001).

750

751 **6. Conclusions**

752

753 We present the AeroCom phase III nitrate study by assessing aerosol simulations of
754 nitrate and ammonium and their precursors with nine global models. Five of the models
755 couple the chemical calculation online with meteorological simulation, and four use
756 archived meteorological fields driving chemistry. To focus on chemical-physical
757 processes behind the diversity of nitrate simulation, all participating models are
758 encouraged to use HTAP2 emission inventory for aerosol and gas emissions from
759 anthropogenic, aircraft, and ship sources. The simulated aerosols of nitrate and
760 ammonium and their precursors are compared among the models and evaluated against
761 various measurements including surface concentrations and dry/wet depositions from
762 surface measurements, and vertical distributions from aircraft measurements.

763

764 All models capture the main features of the distribution of nitrate and ammonium: large
765 surface and column amounts over China, South Asia, Europe, and U.S. These regions are
766 typically densely populated with large NH_3 and NO_x emissions. Many models also show
767 enhanced nitrate and ammonium over the Middle East and continents over the Southern
768 Hemisphere. The former undergoes huge dust pollution and the latter experiences fires
769 that emit both NH_3 and NO_x .

770

771 The diversity of nitrate and ammonium simulations among the models is large: the ratio
772 of the maximum to minimum quantities among the nine models is 13.4 and 4.4 for model
773 simulated global mass burdens of nitrate and ammonium, respectively, and 3.9 and 5.2
774 for the corresponding lifetimes. These values are also larger than those of sulfate: 4.0 for
775 global burden and 3.0 for lifetime. The agreement between models and observations is
776 better for aerosol components than for gas tracers. All models underestimate NH_3 surface
777 mass concentrations but most models overestimate surface HNO_3 concentrations over
778 North America and East Asia. Performance of NH_3 is the worst: this could partially be

779 associated to its relatively lower measurement accuracy, i.e. a loss of ammonia possibly
780 on the filters designed to collect NH₃ (Williams et al., 1992). Among aerosol simulations,
781 model performance based on evaluation of surface mixing ratio and dry/wet depositions
782 is very similar for NH₄⁺ and SO₄²⁻, while slightly worse for NO₃⁻. Models severely
783 underestimate the aerosol concentrations with only a few exceptions when compared with
784 aircraft measurements and this problem is worse over regions impacted by long-range
785 transport than those closer to sources.

786

787 There are many intrinsic reasons for a larger diversity in nitrate simulations among
788 models. Nitrate is involved in much more complicated chemistry: the chemical
789 mechanism needs to handle a multiphase multicomponent solution system. The system
790 sometimes cannot even be solved using the thermodynamic equilibrium approach when
791 coarse mode dust and sea salt particles present. A reasonable nitrate simulation also
792 depends on good simulations of various precursors, such as NH₃, HNO₃, dust and sea
793 salt, although models account for impact of dust and sea salt very differently. Even an
794 accurate simulation of SO₄²⁻ is a prerequisite because SO₄²⁻ surpasses NO₃⁻ at reacting
795 with NH₄⁺.

796

797 The models' intercomparison and model-observation comparison revealed at least two
798 critical issues in nitrate simulation that demand further exploration: NH₃ wet deposition
799 and relative contribution to NO₃⁻ formation via NH₃ and dust/sea salt. The nine
800 participating models adopt very different effective Henry's law constants for NH₃, with
801 one group having a value equal or less than 100 (in pure water) and the other larger than
802 1.e+05 (with pH correction). Sensitivity studies using the GMI model indicated that
803 without pH correction, NH₃ wet deposition decreases massively (from 17.5 to 1.1 Tg),
804 which prolongs atmospheric NH₃ lifetime (from 0.67 to 5.2 days) and enhances its
805 atmospheric burden (from 0.11 to 0.85 Tg), and thus the atmospheric burden of NH₄⁺
806 (from 0.17 to 0.48 Tg) and NO₃⁻ (from 0.26 to 0.97 Tg) as well. These enhanced tracers
807 tend to accumulate in the upper troposphere and close to the tropopause, and are too high
808 when compared with aircraft measurements. Since liquid-phase reaction 2 in Appendix
809 can reach equilibrium quickly within a chemical time step, we recommend including it in
810 accounting for NH₃ solution. Theoretically, a more accurate approach is to combine wet
811 removal with liquid-phase chemistry calculation. In other words, instead of using an
812 implicit calculation of effective Henry's law constant, the gas-liquid phase equilibrium is
813 explicitly calculated based on the chemical mechanism used in the liquid phase. The
814 solution of NH₃ is calculated by solving a set of partial differential equations, which
815 includes not only the gas-liquid phase equilibrium, but also all the important reactions in
816 the liquid phase, as adopted in EMAC model.

817

818 All the models use thermodynamic equilibrium to solve the chemical process of
819 NH₃/NH₄⁺ to NO₃⁻ formation in fine mode aerosols. However, the models adopt very
820 different ways in accounting for the contribution of these reactions on the surface of dust
821 and sea salt particles: some account for both dust and sea salt, some account for only dust
822 or only sea salt, and two models even do not account for ~~any heterogeneous reactions~~
823 ~~and sea salt~~. The methodologies that take dust and sea salt into account are also very
824 different, i.e. together with NH₄⁺ using thermodynamic equilibrium model or simply

825 adopting a first order loss rate on dust and sea salt surfaces. The chemical budget reported
826 by GMI and INCA indicates that the majority (>80%) of global NO_3^- formation is via
827 reaction on dust and sea salt. Two sensitivity experiments using the GMI model by
828 tagging the NO_3^- formation from either $\text{NH}_3/\text{NH}_4^+$ chemistry or heterogeneous reactions
829 on dust and sea salt confirm the critical importance of the latter process, and indicate that
830 the former process is relatively important in remote regions. The importance of NO_3^-
831 formation on dust and sea salt lies also in its determination on nitrate particle size
832 distribution, so that has an implication in air quality and climate studies as well.

833
834 Our work presents a first effort to assess nitrate simulation from chemical (e.g. chemistry
835 among NH_3 , NH_4^+ , NO_3^- , SO_4^{2-} , dust and sea salt) and physical processes (e.g. emission,
836 dry deposition, and wet deposition). A companion study is proposed by AeroCom III
837 nitrate activity to investigate how sensitive ~~is~~ nitrate formation is in response to ~~the~~
838 possible future changes ~~of-in~~ emission and meteorological fields. These perturbation
839 fields include increasing NH_3 emission, decreasing NO_x , SO_x , and dust emissions, and
840 increasing atmospheric temperature and relative humidity. It would be particularly
841 interesting to examine how aerosol pH changes and its influence on atmospheric
842 acid/base gas-particle system ~~during the experiment~~. Future aerosol pH does not
843 necessarily increase with SO_2 emission reduction. Indeed, studies over US southeast
844 indicated that its aerosol has been getting become more acidic over the past decade
845 although SO_2 emission decreased and NH_3 emission stayed constant [Silvern et al., 2017;
846 Weber et al., 2016]. This environment of high aerosol acidity hinders the formation of
847 nitrate aerosol, which only occurs when pH is over ~2 to 3 [Weber et al., 2016]. In
848 addition, understanding why and how the system is insensitive to changing SO_2 level due
849 to buffering of the partitioning of semivolatile NH_3 over regions such as US southeast
850 helps us to gain some insight into how errors in sulfate (and ammonium) may propagate
851 to errors in aerosol nitrate. In particular, the correlation between model predictions and
852 observations for SO_4^{2-} and NH_4^+ is quite poor for some models (Figure 4). ~~-It would~~ also
853 be also interesting to include organic gas/aerosol ~~into~~ the system since they are not only
854 important atmospheric components, but also reduce the uptake of NH_3 . Competition for
855 uptake between NH_3 and organic gases considerably slows down the approach to
856 thermodynamic equilibrium [Silvern et al., 2017]. ~~-Based on the findings of this work,~~
857 modelers should pay particular attention to incorporating dust and sea salt and treating
858 NH_3 wet deposition to improve nitrate simulation. Further evaluation using satellite
859 measurements, such as NH_3 products from IASI and TES, is desired and will be
860 conducted. Such evaluation requires global 3-dimensional high frequency model data.
861 Potential future study also includes estimation of nitrate forcing for climate change.

862 Appendix

863 For some acidic/basic gases, including NH_3 , Henry's law constant is also a function of
864 pH in water (a.k.a effective Henry's law constant). This is because not only does the
865 aqueous chemistry reaction $\text{NH}_3 + \text{H}_2\text{O}$ (equation 1) reach equilibrium within a chemical
866 time step but its product $\text{NH}_3 \cdot \text{H}_2\text{O}$ (equation 2) does as well.



868 Here, NH_4^+ is the ammonium ion and OH^- is the hydroxide ion. The total dissolved
 869 ammonia $[\text{NH}_3^T]$ is given by

$$\begin{aligned} [\text{NH}_3^T] &= [\text{NH}_3 \cdot \text{H}_2\text{O}] + [\text{NH}_4^+] \\ &= p_{\text{NH}_3} H^\ominus \left(1 + \frac{K_{\text{al}}[\text{H}^+]}{K_w} \right) \\ &\approx p_{\text{NH}_3} \left(H^\ominus \frac{K_{\text{al}}[\text{H}^+]}{K_w} \right) \end{aligned} \quad (3)$$

870 Here, p_{NH_3} is the partial pressure of NH_3 , $K_{\text{al}} = [\text{NH}_4^+][\text{OH}^-] / [\text{NH}_3 \cdot \text{H}_2\text{O}] \approx 1.8 \times 10^{-5}$, and
 871 $K_w = 1.0 \times 10^{-14}$ at 298 K in pure water. So the effective Henry's law constant $H^{\ominus*}$ is
 872 inferred from H^\ominus with a correction of pH ($\text{pH} = -\log_{10}[\text{H}^+]$) as

$$H^{\ominus*} = H^\ominus \frac{K_{\text{al}}[\text{H}^+]}{K_w} \quad (4)$$

873

874 **References:**

- 875 Allen, H. M., D. C. Draper, B. R. Ayres, A. Ault, A. Bondy, S. Takahama, R. L. Modini, K. Baumann, E.
 876 Edgerton, C. Knote, A. Laskin, B. Wang, and J. L. Fry, Influence of crustal dust and sea spray
 877 supermicron particle concentrations and acidity on inorganic NO_3 aerosol during the 2013 Southern
 878 Oxidant and Aerosol Study, *Atmos. Chem. Phys.*, 15, 10669–10685, 2015, [www.atmos-chem-](http://www.atmos-chem-phys.net/15/10669/2015/)
 879 [phys.net/15/10669/2015/](http://www.atmos-chem-phys.net/15/10669/2015/), doi:10.5194/acp-15-10669-2015.
- 880 Bauer, S. E., Balkanski, Y., Schulz, M., Hauglustaine, D. A., and Dentener, F.: Global modeling of
 881 heterogeneous chemistry on mineral aerosol surfaces: Influence on tropospheric ozone chemistry and
 882 comparison to observations, *J. Geophys. Res.-Atmos.*, 109, D02304, doi:10.1029/2003jd003868, 2004.
- 883 Bauer, S.E., and D. Koch, 2005: Impact of heterogeneous sulfate formation at mineral dust surfaces on
 884 aerosol loads and radiative forcing in the Goddard Institute for Space Studies general circulation
 885 model. *J. Geophys. Res.*, 110, D17202, doi:10.1029/2005JD005870.
- 886 Bauer, S. E., Koch, D., Unger, N., Metzger, S. M., Shindell, D. T., and Streets, D. G.: Nitrate aerosols
 887 today and in 2030: a global simulation including aerosols and tropospheric ozone, *Atmos. Chem.*
 888 *Phys.*, 7, 5043–5059, doi:10.5194/acp-7-5043-2007, 2007.
- 889 Bauer, S.E., D. Wright, D. Koch, E.R. Lewis, R. McGraw, L.-S. Chang, S.E. Schwartz, and R. Ruedy,
 890 2008: MATRIX (Multiconfiguration Aerosol TRacker of mIXing state): An aerosol microphysical
 891 module for global atmospheric models. *Atmos. Chem. Phys.*, 8, 6603-6035, doi:10.5194/acp-8-6003-
 892 2008.
- 893 Bauer, S. E., K. Tsigaridis, and R. Miller, Significant atmospheric aerosol pollution caused by world food
 894 cultivation, *Geophys. Res. Lett.*, 43, no. 10, 5394-5400, doi:10.1002/2016GL068354, 2016.
- 895 Bessagnet, B. and Rouil, L.: Feedback on and analysis of the PM pollution episode in March 2014,
 896 presentation at 19-th EIONET Workshop on Air Quality Assessment and Management Berne,
 897 Switzerland, 30 September and 1 October 2014, 2014.
- 898 Bey, I, D.J. Jacob, R.M. Yantosca, J.A. Logan, B.D. Field, A.M. Fiore, Q. Li, H.Y. Liu, L.J. Mickley, M.G.
 899 Schultz, 2001: Global modeling of tropospheric chemistry with assimilated meteorology: Model
 900 description and evaluation. *J. Geophys. Res.*, 106, 23073-23078 (2001JD000807).
- 901 Bellouin, N., Rae, J., Jones, A., Johnson, C., Haywood, J., and Boucher, O.: Aerosol forcing in the Climate
 902 Model Intercomparison Project (CMIP5) simulations by HadGEM2-ES and the role of ammonium
 903 nitrate, *J. Geophys. Res.-Atmos.*, 116, D20206, doi:10.1029/2011jd016074, 2011.
- 904 Bernsten, T. K. and Isaksen, I. S. A.: A global three-dimensional chemical transport model for the
 905 troposphere. I. Model description and CO and ozone results, *J. Geophys. Res.-Atmos.*, 102(D17), 21
 906 239–21 280, 1997.
- 907 Bian, H., and C. S. Zender (2003), Mineral dust and global tropospheric chemistry: The relative roles of
 908 photolysis and heterogeneous uptake. *J. Geophys. Res.*, 108, 4672.
- 909 Bian, H., Chin, M., Rodriguez, J. M., Yu, H., Penner, J. E., and Strahan, S., 2009: Sensitivity of aerosol
 910 optical thickness and aerosol direct radiative effect to relative humidity, *Atmos. Chem. Phys.*, 9, 2375-
 911 2386, doi:10.5194/acp-9-2375-2009.

912 Bian, H., Colarco, P. R., Chin, M., Chen, G., Rodriguez, J. M., Liang, Q., Blake, D., Chu, D. A.,
913 da Silva, A., Darmenov, A. S., Diskin, G., Fuelberg, H. E., Huey, G., Kondo, Y., Nielsen, J. E.,
914 Pan, X., and Wisthaler, A.: Source attributions of pollution to the Western Arctic during the NASA
915 ARCTAS field campaign, *Atmos. Chem. Phys.*, 13, 4707-4721, doi:10.5194/acp-13-4707-2013, 2013.
916 Bouwman, A.F., Lee, D.S., Asman, W.A.H., Dentener, F.J., Van Der Hoek, K.W. and J.G.J. Olivier (1997).
917 A Global High-Resolution Emission Inventory for Ammonia, *Global Biogeochemical Cycles*, 11:4,
918 561-587. <http://www.rivm.nl/>.

919 Chin, M., P. Ginoux, S. Kinne, B. N. Holben, B. N. Duncan, R. V. Martin, J. A. Logan, A. Higurashi, and
920 T. Nakajima, 2002: Tropospheric aerosol optical thickness from the GOCART model and comparisons
921 with satellite and sun photometer measurements, *J. Atmos. Sci.* 59, 461-483.

922 [Cubison, M. J., Ortega, A. M., Hayes, P. L., Farmer, D. K., Day, D., Lechner, M. J., Brune, W. H., Apel,
923 E., Diskin, G. S., Fisher, J. A., Fuelberg, H. E., Hecobian, A., Knapp, D. J., Mikoviny, T., Riemer, D.,
924 Sachse, G. W., Sessions, W., Weber, R. J., Weinheimer, A. J., Wisthaler, A., and Jimenez, J. L.:
925 Effects of aging on organic aerosol from open biomass burning smoke in aircraft and laboratory
926 studies, *Atmos. Chem. Phys.*, 11, 12049–12064, doi:10.5194/acp-11-12049-2011, 2011.](#)

927 [Davis, J. M., P. M. Bhawe, and K. M. Foley \(2008\). Parameterization of N2O5 reaction probabilities on the
928 surface of particles containing ammonium, sulfate and nitrate, *Atmos. Chem. Phys.*, 8, 5295 – 5311.](#)

929 [Cubison, M.J., A.M. Ortega, P.L. Hayes, D.K. Farmer, D. Day, M.J. Lechner, W.H. Brune, E. Apel, G.S.
930 Diskin, J.A. Fisher, H.E. Fuelberg, A. Hecobian, D.J. Knapp, T. Mikoviny, D. Riemer, G.W. Sachse,
931 W. Sessions, R.J. Weber, A.J. Weinheimer, A. Wisthaler, and J.L. Jimenez \(2011\), Effects of Aging on
932 Organic Aerosol from Open Biomass Burning Smoke in Aircraft & Lab Studies, *Atmos. Chem. and
933 Phys. Disc.* 11, 12103–12140, doi:10.5194/acpd-11-12103-2011.](#)

934 DeCarlo, P. F., Kimmel, J. R., Trimborn, A., Northway, M. J., Jayne, J. T., Aiken, A. C., Gonin, M.,
935 Fuhrer, K., Horvath, T., Docherty, K. S., Worsnop, D. R., and Jimenez, J. L.: Field-deployable, high-
936 resolution, time-of-flight aerosol mass spectrometer, *Anal. Chem.*, 78(24), 8281–8289, 2006.

937 Dentener, F. J., G. R. Carmichael, Y. Zhang, J. Lelieveld, and P. J. Crutzen, Role of mineral aerosol as a
938 reactive surface in the global troposphere, *J. Geophys. Res.*, 101, 22,869-22889, 1996.

939 [Dentener, F. and Crutzen, P.: Reaction of NO on Tropospheric Aerosols: Impact on the Global
940 Distributions of NO, O, and OH, *J. Geophys. Res.*, 98, 7149–7163, doi:10.1029/92JD02979, 1993.](#)

941 Dentener, F., Kinne, S., Bond, T., Boucher, O., Cofala, J., Generoso, S., Ginoux, P., Gong, S., Hoelzemann,
942 J. J., Ito, A., Marelli, L., Penner, J. E., Putaud, J.-P., Textor, C., Schulz, M., van der Werf, G. R., and
943 Wilson, J.: Emissions of primary aerosol and precursor gases in the years 2000 and 1750 prescribed
944 data-sets for AeroCom, *Atmos. Chem. Phys.*, 6, 4321–4344, doi:10.5194/acp-6-4321-2006, 2006.

945 [Evans, M. J. and Jacob, D. J.: Impact of new laboratory studies of N2O5 hydrolysis on global model
946 budgets of tropospheric nitrogen oxides, ozone and OH, *Geophys. Res. Lett.*, 32, L09813,
947 doi:10.1029/2005GL022469, 2005.](#)

948 Ensbjerg, J. J., Craven, J. S., Metcalf, A. R., Allan, J. D., Angevine, W. M., Bahreini, R., Brioude, J., Cai,
949 C., Coe, H., de Gouw, J. A., Ellis, R. A., Flynn, J. H., Haman, C. L., Hayes, P. L., Jimenez, J. L.,
950 Lefer, B. L., Middlebrook, A. M., Murphy, J. G., Neuman, J. A., Nowak, J. B., Roberts, J. M., Stutz, J.,
951 Taylor, J. W., Veres, P. R., Walker, J. M., and Seinfeld, J. H.: Inorganic and black carbon aerosols in
952 the Los Angeles Basin during CalNex, *Journal of Geophysical Research-Atmospheres*, 118, 1777-
953 1803, 2013.

954 Fairlie, T. D., Jacob, D. J., Dibb, J. E., Alexander, B., Avery, M. A., van Donkelaar, A., and Zhang, L.:
955 Impact of mineral dust on nitrate, sulfate, and ozone in transpacific Asian pollution plumes, *Atmos.*
956 *Chem. Phys.*, 10, 3999–4012, doi:10.5194/acp-10-3999-2010, 2010.

957 Feng, Y. and Penner, J. E.: Global modeling of nitrate and ammonium: Interaction of aerosols and
958 tropospheric chemistry, *J. Geophys. Res.-Atmos.*, 112, D01304, doi:10.1029/2005jd006404, 2007.

959 Fenn, M. E., M. A. Poth, D. W. Johnson, Evidence for nitrogen saturation in the San Bernardino Mountains
960 in southern California, *Forest Ecology and Management*, Volume 82, Issues 1–3, April 1996, Pages
961 211-230.

962 Fitzgerald, J. W. (1975), Approximation formulas for equilibrium size of an aerosol particle as a function
963 of its dry size and composition and ambient relative humidity, *J. Appl. Meteorol.*, 14(6), 1044-1049.

964 Fowler, Z. K., M. B. Adams, W. T. Peterjohn, Will more nitrogen enhance carbon storage in young forest
965 stands in central Appalachia? *Forest Ecology and Management*, Volume 337, Pages 144–152, 1
966 February 2015.

967 Galloway, J. N., Dentener, F. J., Capone, D. G., Boyer, E. W., Howarth, R. W., Seitzinger, S. P., Asner, G.
968 P., Cleveland, C. C., Green, P. A., Holland, E. A., Karl, D. M., Michaels, A. F., Porter, J. H.,
969 Townsend, A. R. and Vorosmarty, C. J.: Nitrogen cycles: Past, present, and future, *Biogeochemistry*,
970 70, 153–226, 2004.

971 Ginoux, P., M. Chin, I. Tegen, J. Prospero, B. Holben, O. Dubovik, and S.-J. Lin, 2001: Sources and global
972 distributions of dust aerosols simulated with the GOCART model, *J. Geophys. Res.*, 106, 20,255-
973 20,273.

974 Grieshop, A. P., Robinson, A. L., Duplissy, J., Smith, J. D., Wilson, K. R., Lanz, V. A., Hueglin, C., Sun,
975 Y. L., Tian, J., Laaksonen, A., Raatikainen, T., Rautiainen, J., Vaattovaara, P., Ehn, M., Kulmala, M.,
976 Tomlinson, J. M., Collins, D. R., Cubison, M. J., Dunlea, E. J., Huffman, J. A., Onasch, T. B., Alfarra,
977 M. R., Williams, P. I., Bower, K., Kondo, Y., Schneider, J., Drewnick, F., Borrmann, S., Weimer, S. S.,
978 Demerjian, K., Salcedo, D., Cottrell, L., Griffin, R., Takami, A., Miyoshi, T., Hatakeyama, S.,
979 Shimono, A., Sun, J. Y., Zhang, Y. M., Dzepina, K., Kimmel, J. R., Sueper, D., Jayne, J. T., Herndon,
980 S. C., Trimborn, A. M., Williams, L. R., Wood, E. C., Middlebrook, A. M., Kolb, C. E., Baltensperger,
981 U., and Worsnop, D. R.: Evolution of organic aerosols in the atmosphere, *Science*, 326, 1525–1529,
982 2009.

983 Hansell, D.A., Follows, M.J., 2008. Nitrogen in the Atlantic Ocean. In: Mullholland, M., Bronk, D.,
984 Capone, D., Carpenter, E. (Eds.), *Nitrogen in the Marine Environment*, second ed. Academic Press, pp.
985 597–630.

986 Hauglustaine, D. A., Hourdin, F., Walters, S., Jourdain, L., Filiberti, M.-A., Lamarque, J.-F., and Holland,
987 E. A.: Interactive chemistry in the Laboratoire de Météorologie Dynamique general circulation model:
988 description and background tropospheric chemistry evaluation, *J. Geophys. Res.*, 109, D04314,
989 doi:10.1029/2003JD003957, 2004.

990 Hauglustaine, D. A., Balkanski, Y., and Schulz, M.: A global model simulation of present and future
991 nitrate aerosols and their direct radiative forcing of climate, *Atmos. Chem. Phys.*, 14, 11031–11063,
992 doi:10.5194/acp-14-11031-2014, 2014.

993 Haywood, J., Bush, M., Abel, S., Claxton, B., Coe, H., Crosier, J., Harrison, M., Macpherson, B., Naylor,
994 M., and Osborne, S.: Prediction of visibility and aerosol within the operational Met Office Unified
995 Model II?: Validation of model performance using observational data, *Q. J. Roy. Meteorol. Soc.*, 134,
996 1817–1832, doi:10.1002/qj.275, 2008.

997 Heald, C. L., Collett Jr., J. L., Lee, T., Benedict, K. B., Schwandner, F. M., Li, Y., Clarisse, L., Hurtmans,
998 D. R., Van Damme, M., Clerbaux, C., Coheur, P.-F., Philip, S., Martin, R. V., and Pye, H. O. T.:
999 Atmospheric ammonia and particulate inorganic nitrogen over the United States, *Atmos. Chem. Phys.*,
1000 12, 10295–10312, doi:10.5194/acp-12-10295-2012, 2012.

1001 Hess, M., P. Koepke and I. Schult, Optical properties of aerosols and clouds: The software package OPAC.
1002 *Bull. Amer. Meteorol. Soc.*, 79(5): 831-844, 1998.

1003 [Hodzic, A., R. Vautard, P. Chazette, L. Menut, and B. Bessagnet, Aerosol chemical and optical properties](#)
1004 [over the Paris area within ESQUIF project. *Atmos. Chem. Phys.*, 6, 3257 – 3280, 2006a.](#)

1005 [Hodzic, A., Bessagnet, B., and Vautard, R.: A model evaluation of coarse-mode nitrate heterogeneous](#)
1006 [formation on dust particles. *Atmos. Environ.*, 40 4158–4171, 2006b.](#)

1007 Huffman, J. A., J. T. Jayne, F. Drewnick, A. C. Aiken, T. Onasch, D. R. Worsnop, and J. L. Jimenez,
1008 Design, Modeling, Optimization, and Experimental Tests of a Particle Beam Width Probe for the
1009 Aerodyne Aerosol Mass Spectrometer, *Aerosol Sci Technol.* 39, 1143-1163, 2005.

1010 Huneus, N., M. Schulz, Y. Balkanski, J. Griesfeller, S. Kinne, J. Prospero, S. Bauer, O. Boucher, M. Chin,
1011 F. Dentener, T. Diehl, R. Easter, D. Fillmore, S. Ghan, P. Ginoux, A. Grini, L. Horowitz, D. Koch,
1012 M.C. Krol, W. Landing, X. Liu, N. Mahowald, R.L. Miller, J.-J. Morcrette, G. Myhre, J.E. Penner, J.P.
1013 Perlwitz, P. Stier, T. Takemura, and C. Zender, 2011: Global dust model intercomparison in AeroCom
1014 phase I. *Atmos. Chem. Phys.*, 11, 7781-7816, doi:10.5194/acp-11-7781-2011.

1015 IPCC: (Intergovernmental Panel on Climate Change): The physical science basis. Contribution of working
1016 group I to the fifth assessment report of the intergovernmental panel on climate change. T.F. Stocker, D.
1017 Qin, G.-K. Plattner, M. Tignor, S.K. Allen, J. Boschung, A. Nauels, Y. Xia, V. Bex, and P.M. Midgley
1018 (eds.). Cambridge University Press, Cambridge, United Kingdom and New York, NY, USA, 2013.
1019 2013.

1020 Jimenez, J. L., Canagaratna, M. R., Donahue, N. M., Prevot, A. S. H., Zhang, Q., Kroll, J. H., DeCarlo, P.
1021 F., Allan, J. D., Coe, H., Ng, N. L., Aiken, A. C., Docherty, K. S., Ulbrich, I. M.,

1022 [Jacob, D. J., Crawford, J. H., Maring, H., Clarke, A. D., Dibb, J. E., Emmons, L. K., Ferrare, R. A.,](#)
1023 [Hostetler, C. A., Russell, P. B., Singh, H. B., Thompson, A. M., Shaw, G. E., McCauley, E., Pederson,](#)
1024 [J. R., and Fisher, J. A.: The Arctic Research of the Composition of the Troposphere from Aircraft and](#)
1025 [Satellites \(ARCTAS\) mission: design, execution, and first results, *Atmos. Chem. Phys.*, **10**, 5191–](#)
1026 [5212, doi:10.5194/acp-10-5191-2010, 2010.](#)
1027 [Jöckel, P., Kerkweg, A., Pozzer, A., Sander, R., Tost, H., Riede, H., Baumgaertner, A., Gromov, S., and](#)
1028 [Kern, B.: Development cycle 2 of the Modular Earth Submodel System \(MESSy2\), *Geosci. Model*](#)
1029 [Dev.](#), **3**, 717–752, <https://doi.org/10.5194/gmd-3-717-2010>, 2010.
1030 [Jacob, D. J., Crawford, J. H., Maring, H., Clarke, A. D., Dibb, J. E., Emmons, L. K., Ferrare, R. A.,](#)
1031 [Hostetler, C. A., Russell, P. B., Singh, H. B., Thompson, A. M., Shaw, G. E., McCauley, E., Pederson,](#)
1032 [J. R., and Fisher, J. A.: The Arctic Research of the Composition of the Troposphere from Aircraft and](#)
1033 [Satellites \(ARCTAS\) mission: design, execution, and first results, *Atmos. Chem. Phys.*, **10**, 5191–](#)
1034 [5212, doi:10.5194/acp-10-5191-2010, 2010.](#)
1035 Janssens-Maenhout, G., Crippa, M., Guizzardi, D., Dentener, F., Muntean, M., Pouliot, G., Keating, T.,
1036 Zhang, Q., Kurokawa, J., Wankmüller, R., Denier van der Gon, H., Kuenen, J. J. P., Klimont, Z., Frost,
1037 G., Darras, S., Koffi, B., and Li, M.: HTAP_v2.2: a mosaic of regional and global emission grid maps
1038 for 2008 and 2010 to study hemispheric transport of air pollution, *Atmos. Chem. Phys.*, **15**, 11411–
1039 11432, doi:10.5194/acp-15-11411-2015, 2015
1040 Jöckel, P., Kerkweg, A., Pozzer, A., Sander, R., Tost, H., Riede, H., Baumgaertner, A., Gromov, S., and
1041 Kern, B.: Development cycle 2 of the Modular Earth Submodel System (MESSy2), *Geosci. Model*
1042 *Dev.*, **3**, 717–752, doi:10.5194/gmd-3-717-2010, 2010.
1043 John, W., S. M. Wall, J. L. Ondo, and W. Winklmayr (1989), Acidic-aerosol size distributions during
1044 SCAQS (Southern California Air Quality Study), final report, Rep. CA/DOH/AIHL/SP-51, Calif. Air
1045 Resour. Board, Sacramento.
1046 Kanakidou, M., R.A. Duce, J.M. Prospero, A.R. Baker, C. Benitez-Nelson, F.J. Dentener, K.A. Hunter,
1047 P.S. Liss, N. Mahowald, G.S. Okin, M. Sarin, K. Tsigaridis, M. Uematsu, L.M. Zamora, and T. Zhu,
1048 2012: Atmospheric fluxes of organic N and P to the global ocean. *Glob. Biogeochem. Cycles*, **26**,
1049 GB3026, doi:10.1029/2011GB004277.
1050 Kanakidou, M., S. Myriokefalitakis, N. Daskalakis, G. Fanourgakis, A. Nenes, A. Baker, K. Tsigaridis, and
1051 N. Mihalopoulos, 2016: Past, present and future atmospheric nitrogen deposition. *J. Atmos. Sci.*, **73**,
1052 no. 5, 2039–2047, doi:10.1175/JAS-D-15-0278.1.
1053 Karydis, V. A., Tsimpidi, A. P., Fountoukis, C., Nenes, A., Zavala, M., Lei, W., Molina, L. T., and Pandis,
1054 S. N.: Simulating the fine and coarse inorganic particulate matter concentrations in a polluted
1055 megacity, *Atmospheric Environment*, **44**, 608–620, 2010.
1056 Karydis, V. A., Tsimpidi, A. P., Lei, W., Molina, L. T., and Pandis, S. N.: Formation of semivolatile
1057 inorganic aerosols in the Mexico City Metropolitan Area during the MILAGRO campaign,
1058 *Atmospheric Chemistry and Physics*, **11**, 13305–13323, 2011.
1059 Karydis, V. A., A. P. Tsimpidi, A. Pozzer, M. Astitha, and J. Lelieveld, 2016: Effects of mineral dust on
1060 global atmospheric nitrate concentrations. *Atmos. Chem. Phys.*, **16**, 1491–1509, doi:10.5194/acp-16-
1061 1491-2016.
1062 Kim, Y. P., Seinfeld, J. H., and Saxena, P.: Atmospheric gas–aerosol equilibrium I. Thermodynamic model,
1063 *Aerosol Sci. Technol.*, **19**, 157–181, 1993.
1064 Kim, D., M. Chin, H. Yu, T. Diehl, Q. Tan, R.A. Kahn, K. Tsigaridis, S.E. Bauer, T. Takemura, L. Pozzoli,
1065 N. Bellouin, M. Schulz, S. Peyridieu, A. Chédin, and B. Koffi, 2014: Sources, sinks, and transatlantic
1066 transport of North African dust aerosol: A multi-model analysis and comparison with remote-sensing
1067 data. *J. Geophys. Res. Atmos.*, **119**, no. 10, 6259–6277, doi:10.1002/2013JD021099.
1068 Kinne, S., Schulz, M., Textor, C., Guibert, S., Balkanski, Y., Bauer, S. E., Bernsten, T., Berglen, T. F.,
1069 Boucher, O., Chin, M., Collins, W., Dentener, F., Diehl, T., Easter, R., Feichter, J., Fillmore, D., Ghan,
1070 S., Ginoux, P., Gong, S., Grini, A., Hendricks, J., Herzog, M., Horowitz, L., Isaksen, I., Iversen, T.,
1071 Kirkevåg, A., Kloster, S., Koch, D., Kristjansson, J. E., Krol, M., Lauer, A., Lamarque, J. F., Lesins,
1072 G., Liu, X., Lohmann, U., Montanaro, V., Myhre, G., Penner, J., Pitari, G., Reddy, S., Seland, O.,
1073 Stier, P., Takemura, T., and Tie, X.: An AeroCom initial assessment – optical properties in aerosol
1074 component modules of global models, *Atmos. Chem. Phys.*, **6**, 1815–1834, doi:10.5194/acp-6-1815-
1075 2006, 2006.
1076 Koch, D., M. Schulz, S. Kinne, C. McNaughton, J.R. Spackman, T.C. Bond, Y. Balkanski, S. Bauer, T.
1077 Bernsten, O. Boucher, M. Chin, A. Clarke, N. De Luca, F. Dentener, T. Diehl, O. Dubovik, R. Easter,

1078 D.W. Fahey, J. Feichter, D. Fillmore, S. Freitag, S. Ghan, P. Ginoux, S. Gong, L. Horowitz, T. Iversen,
 1079 A. Kirkevåg, Z. Klimont, Y. Kondo, M. Krol, X. Liu, R.L. Miller, V. Montanaro, N. Moteki, G.
 1080 Myhre, J.E. Penner, J.P. Perlwitz, G. Pitari, S. Reddy, L. Sahu, H. Sakamoto, G. Schuster, J.P.
 1081 Schwarz, Ø. Seland, P. Stier, N. Takegawa, T. Takemura, C. Textor, J.A. van Aardenne, and Y. Zhao,
 1082 2009: Evaluation of black carbon estimations in global aerosol models. *Atmos. Chem. Phys.*, 9, 9001-
 1083 9026, doi:10.5194/acp-9-9001-2009.
 1084 Kinnison, D. E., P. S. Connell, J. Rodriguez, D. B. Considine, D. A. Rotman, J. Tannahill, R. Ramarosan,
 1085 A. Douglass, S. Baughcum, L. Coy, P. Rasch, D. Waugh, 2001: The Global Modeling Initiative
 1086 assessment model: Application to high-speed civil transport perturbation, *J. Geophys. Res.*, 106, 1693-
 1087 1712.
 1088 Lacis, A. A., Refractive Indices of Three Hygroscopic Aerosols and their Dependence on Relative
 1089 Humidity, http://gacp.giss.nasa.gov/data_sets/lacis/introduction.pdf.
 1090 Lamarque, J.-F., J. T. Kiehl, G. P. Brasseur, T. Butler, P. Cameron-Smith, et al. (2005), Assessing future
 1091 nitrogen deposition and carbon cycle feedback using a multimodel approach : Analysis of nitrogen
 1092 deposition, *J. of Geophys. Res.*, Vol. 110, D19303, doi: 10.1029/2005JD005825.
 1093 Lee, T., X.-Y. Yu, B. Ayres, S. M. Kreidenweis, W. C. Malm, J. L. Collett Jr., Observations of fine and
 1094 coarse particle nitrate at several rural locations in the United States, *Atmospheric Environment* 42,
 1095 2720–2732, 2008.
 1096 Li, J., W.-C. Wang, H. Liao, and W. Chang. 2014. Past and future direct radiative forcing of nitrate aerosol
 1097 in East Asia. *Theor. Appl. Climatol.* 1–14. doi:10.1007/s00704-014-1249-1.
 1098 Liao, H., P. J. Adams, S. H. Chung, J. H. Seinfeld, L. J. Mickley, and D. J. Jacob (2003), Interactions
 1099 between tropospheric chemistry and aerosols in a unified general circulation model, *J. Geophys. Res.*,
 1100 108(D1), 4001, doi:10.1029/2001JD001260.
 1101 Liu, X., J. E. Penner, S. J. Ghan, and M. Wang, 2007: Inclusion of Ice Microphysics in the NCAR
 1102 Community Atmospheric Model Version 3 (CAM3). *J. Climate*, 20, 4526-4547.
 1103 Liu, Y., G. Gibson, C. Cain, H. Wang, G. Grassian, and A. Laskin (2008) Kinetics of Heterogeneous
 1104 Reaction of CaCO₃ Particles with Gaseous HNO₃ over a Wide Range of Humidity, *J. Physical
 1105 Chemistry A*, doi:10.1021/jp076169h
 1106 Malm, W. C., Schichtel, B. A., Pitchford, M. L., Ashbaugh, L. L., and Eldred, R. A.: Spatial and monthly
 1107 trends in speciated fine particle concentration in the United States, *J. Geophys. Res. Atmos.*, 109(D3),
 1108 D03306, doi:10.1029/2003/JD003739, 2004.
 1109 Metzger, S., F. Dentener, S. Pandis, and J. Lelieveld (2002), Gas/aerosol partitioning: 1. A computationally
 1110 efficient model, *J. of Geophys. Res.* Vol. 107, No. D16, 4312, 10.1029/2001JD001102.
 1111 Mezuman, K., S.E. Bauer, and K. Tsigaridis, 2016: Evaluating secondary inorganic aerosols in three
 1112 dimensions. *Atmos. Chem. Phys.*, 16, 10651-10669, doi:10.5194/acp-16-10651-2016.
 1113 Milegroet, H. Van and D. W. Cole, The Impact of Nitrification on Soil Acidification and Cation Leaching
 1114 in a Red Alder Ecosystem, ACSESS, Alliance of Crop, Soil, and Environmental Science Societies,
 1115 doi:10.2134/jeq1984.00472425001300040015x ,1984
 1116 Myhre, G., A. Grini, and S. Metzger (2006), Modeling of nitrate and ammonium-containing aerosols
 1117 in presence of sea salt, *Atmos. Chem. Phys.*, 6, 4809-4821, www.atmos-chem-phys.net/6/4809/2006/.
 1118 Myhre, G., B. H., Samset, M. Schulz, Y. Balkanski, S. Bauer, T. K. Berntsen, H. Bian, N. Bellouin, M.
 1119 Chin, T. Diehl, R. C. Easter, J. Feichter, S. J. Ghan, D. Hauglustaine, T. Iversen, S. Kinne, A.
 1120 Kirkevåg, J.-F. Lamarque, G. Lin, X. Liu, G. Luo, X. Ma, J. E. Penner, P. J. Rasch, Ø. Seland, R. B.
 1121 Skeie, P. Stier, T. Takemura, K. Tsigaridis, Z. Wang, L. Xu, H. Yu, F. Yu, J.-H. Yoon, K. Zhang, H.
 1122 Zhang, and C. Zhou, Radiative forcing of the direct aerosol effect from AeroCom Phase II simulations,
 1123 *Atmos. Chem. Phys.*, 13, 1853-1877, doi:10.5194/acp-13-1853-2013, 2013.
 1124 Nowak, J., J. B., Weinheimer, A. J., Hoff, R. M., Berkoff, T. A., Beyersdorf, A. J., Olson, J., Crawford, J.
 1125 H., and Cohen, R. C.: On the effectiveness of nitrogen oxide reductions as a control over ammonium
 1126 nitrate aerosol, *Atmos. Chem. Phys.*, 16, 2575–2596, doi:10.5194/acp-16-2575-2016, 2016
 1127 Paulot, F., Ginoux, P., Cooke, W. F., Donner, L. J., Fan, S., Lin, M.-Y., Mao, J., Naik, V., and Horowitz, L.
 1128 W.: Sensitivity of nitrate aerosols to ammonia emissions and to nitrate chemistry: implications for
 1129 present and future nitrate optical depth, *Atmos. Chem. Phys.*, 16, 1459–1477, doi:10.5194/acp-16-
 1130 1459-2016, <http://www.atmos-chem-phys.net/16/1459/2016/>, 2016.
 1131 Phoenix, G., W. K. Hicks, S. Cinderby, J. C. I. Kuylenstierna, W. D. Stock, et al. (2006), Atmospheric
 1132 nitrogen deposition in world biodiversity hotspots: the need for a greater global perspective in

1133 assessing N deposition impacts, *Global Change Biology*, 12, 470-476, doi: 10.1111/j.1365-
 1134 2486.2006.01104.x.
 1135 Prentice, M. J., et al. (2001), The carbon cycle and atmospheric carbon dioxide, in *Climate Change 2001*,
 1136 pp. 184-237, Cambridge Univ. Press, New York.
 1137 Pringle, K. J., Tost, H., Message, S., Steil, B., Giannadaki, D., Nenes, A., Fountoukis, C., Stier, P., Vignati,
 1138 E., and Lelieveld, J.: Description and evaluation of GMXe: a new aerosol submodel for global
 1139 simulations (v1), *Geoscientific Model Development*, 3, 391-412, 2010.
 1140 Pusede, S. E., Duffey, K. C., Shusterman, A. A., Saleh, A., Laughner, J. L., Wooldridge, P. J., Zhang, Q.,
 1141 Parworth, C. L., Kim, H., Capps, S. L., Valin, L. C., Cappa, C. D., Fried, A., Walega, Riemer, N., H.
 1142 Vogel, B. Vogel, B. Schell, I. Ackermann, C. Kessler, and H. Hass (2003), Impact of the
 1143 heterogeneous hydrolysis of N₂O₅ on chemistry and nitrate aerosol formation in the lower troposphere
 1144 under photosmog conditions, *J. Geophys. Res.*, 108(D4), 4144, doi:10.1029/2002JD002436.
 1145 Sander, S. P., J. Abbatt, J. R. Barker, J. B. Burkholder, R. R. Friedl, D. M. Golden, R. E. Huie, C. E. Kolb,
 1146 M. J. Kurylo, G. K. Moortgat, V. L. Orkin and P. H. Wine "Chemical Kinetics and Photochemical
 1147 Data for Use in Atmospheric Studies, Evaluation No. 17," JPL Publication 10-6, Jet Propulsion
 1148 Laboratory, Pasadena, 2011 <http://jpldataeval.jpl.nasa.gov>.
 1149 Saxena, P., Hudischekskyj, A. B., Seigneur, C., and Seinfeld, J. H., A comparative study of
 1150 equilibrium approaches to the chemical characterization of secondary aerosols, *Atmos. Environ.*
 1151 20:1471- 1483, 1986.
 1152 Schaap, M., Müller, K., & Ten Brink, H. M. (2002). Constructing the European aerosol nitrate
 1153 concentration field from quality analysed data. *Atmospheric Environment*, 36(8), 1323-1335.
 1154 Schaap, M., van Loon, M., ten Brink, H. M., Dentener, F. J., and Builtjes, P. J. H.: Secondary
 1155 inorganic aerosol simulations for Europe with special attention to nitrate, *Atmos. Chem. Phys.*, 4,
 1156 857-874, doi:10.5194/acp-4-857-2004, 2004.
 1157 Schmidt, G.A., M. Kelley, L. Nazarenko, R. Ruedy, G.L. Russell, I. Aleinov, M. Bauer, S.E. Bauer,
 1158 M.K. Bhat, R. Bleck, V. Canuto, Y.-H. Chen, Y. Cheng, T.L. Clune, A. Del Genio, R. de
 1159 Fainchtein, G. Faluvegi, J.E. Hansen, R.J. Healy, N.Y. Kiang, D. Koch, A.A. Lacis, A.N.
 1160 LeGrande, J. Lerner, K.K. Lo, E.E. Matthews, S. Menon, R.L. Miller, V. Oinas, A.O. Olosolo, J.P.
 1161 Perlwitz, M.J. Puma, W.M. Putman, D. Rind, A. Romanou, M. Sato, D.T. Shindell, S. Sun, R.A.
 1162 Syed, N. Tausnev, K. Tsigaridis, N. Unger, A. Voulgarakis, M.-S. Yao, and J. Zhang, 2014:
 1163 Configuration and assessment of the GISS ModelE2 contributions to the CMIP5 archive. *J. Adv.*
 1164 *Model. Earth Syst.*, 6, no. 1, 141-184, doi:10.1002/2013MS000265.
 1165 Schulz, M., Textor, C., Kinne, S., Balkanski, Y., Bauer, S., Bernsten, T., Berglen, T., Boucher, O.,
 1166 Dentener, F., Guibert, S., Isaksen, I. S. A., Iversen, T., Koch, D., Kirkevåg, A., Liu, X.,
 1167 Montanaro, V., Myhre, G., Penner, J. E., Pitari, G., Reddy, S., Seland, Ø., Stier, P., and
 1168 Takemura, T.: Radiative forcing by aerosols as derived from the AeroCom present-day and pre-
 1169 industrial simulations, *Atmos. Chem. Phys.*, 6, 5225–5246, doi:10.5194/acp-6-5225-2006, 2006.
 1170 Schutgens, N. A. J., Gryspeerd, E., Weigum, N., Tsyro, S., Goto, D., Schulz, M. and Stier, P.: Will a
 1171 perfect model agree with perfect observations? The impact of spatial sampling, *Atmos. Chem.*
 1172 *Phys.*, 16(10), 6335-6353, 2016.
 1173 Shindell, D. T., Faluvegi, G., and Bell, N.: Preindustrial-to-present-day radiative forcing by
 1174 tropospheric ozone from improved simulations with the GISS chemistry-climate GCM, *Atmos.*
 1175 *Chem. Phys.*, 3, 1675–1702, 2003.
 1176 Silvern, R. F., Jacob, D. J., Kim, P. S., Marais, E. A., Turner, J. R., Campuzano-Jost, P., and
 1177 Jimenez, J. L.: Inconsistency of ammonium–sulfate aerosol ratios with thermodynamic
 1178 models in the eastern US: a possible role of organic aerosol, *Atmos. Chem. Phys.*, 17, 5107-
 1179 5118, 10.5194/acp-17-5107-2017, 2017.
 1180 Simpson, D., Benedictow, A., Berge, H., Bergström, R., Emberson, L. D., Fagerli, H., Flechard, C. R.,
 1181 Hayman, G. D., Gauss, M., Jonson, J. E., Jenkin, M. E., Nyíri, A., Richter, C., Semeena, V. S., Tsyro,
 1182 S., Tuovinen, J. P., Valdebenito, A., and Wind, P.: The EMEP MSC-W chemical transport model -
 1183 technical description, *Atmos. Chem. Phys.*, 12, 7825-7865, 10.5194/acp-12-7825-2012, 2012.
 1184 Song, C. H., and G. R. Carmichael, Gas-particle partitioning of nitric acid modulated by alkaline aerosol, *J.*
 1185 *Atmos. Chem.*, 40, 1–22, 2001.

1186 [Søvde, O. A., Prather, M. J., Isaksen, I. S. A., Berntsen, T. K., Stordal, F., Zhu, X., Holmes, C. D., and Hsu,](#)
1187 [J.: The chemical transport model Oslo CTM3. *Geosci. Model Dev.*, 5, 1441-1469,](#)
1188 <https://doi.org/10.5194/gmd-5-1441-2012>, 2012.

1189 Strahan, S. E., Duncan, B. N., and Hoor, P.: Observationally derived transport diagnostics for the
1190 lowermost stratosphere and their application to the GMI chemistry and transport model, *Atmos. Chem.*
1191 *Phys.*, 7, 2435-2445, doi:10.5194/acp-7-2435-2007, 2007.

1192 Sudo, K., M. Takahashi, J. Kurokawa, and H. Akimoto, CHASER: A global chemical model of the
1193 troposphere, 1. Model description, *J. Geophys. Res.*, 107(D17), 4339, doi:10.1029/2001JD001113,
1194 2002.

1195 Takiguchi, Y., A. Takami, Y. Sadanaga, X. Lun, A. Shimizu, I. Matsui, N. Sugimoto, W. Wang, H.
1196 Bandow, and S. Hatakeyama (2008), Transport and transformation of total reactive nitrogen over the
1197 East China Sea, *J. Geophys. Res.*, 113, D10306, doi:10.1029/2007JD009462.

1198 Textor, C., Schulz, M., Guibert, S., Kinne, S., Balkanski, Y., Bauer, S., Berntsen, T., Berglen, T., Boucher,
1199 O., Chin, M., Dentener, F., Diehl, T., Easter, R., Feichter, H., Fillmore, D., Ghan, S., Ginoux, P.,
1200 Gong, S., Grini, A., Hendricks, J., Horowitz, L., Huang, P., Isaksen, I., Iversen, I., Kloster, S., Koch,
1201 D., Kirkevåg, A., Kristjansson, J. E., Krol, M., Lauer, A., Lamarque, J. F., Liu, X., Montanaro, V.,
1202 Myhre, G., Penner, J., Pitari, G., Reddy, S., Seland, Ø., Stier, P., Takemura, T., and Tie, X.: Analysis
1203 and quantification of the diversities of aerosol life cycles within AeroCom, *Atmos. Chem. Phys.*, 6,
1204 1777–1813, doi:10.5194/acp-6-1777-2006, 2006.

1205 Tost, H., Jöckel, P., Kerkweg, A., Sander, R., and Lelieveld, J.: Technical note: A new comprehensive
1206 SCAVenging submodel for global atmospheric chemistry modelling, *Atmos. Chem. Phys.*, 6, 565-574,
1207 doi:10.5194/acp-6-565-2006, 2006.

1208 Trail, M., Tsimpidi, A. P., Liu, P., Tsigaridis, K., Rudokas, J., Miller, P., Nenes, A., Hu, Y., and Russell, A.
1209 G.: Sensitivity of air quality to potential future climate change and emissions in the United States and
1210 major cities, *Atmospheric Environment*, 94, 552-563, 2014.

1211 Trump, E. R., Fountoukis, C., Donahue, N. M., and Pandis, S. N.: Improvement of simulation of fine
1212 inorganic PM levels through better descriptions of coarse particle chemistry, *Atmospheric*
1213 *Environment*, 102, 274-281, 2015.

1214 Tsigaridis, K., Daskalakis, N., Kanakidou, M., Adams, P. J., Artaxo, P., Bahadur, R., Balkanski, Y.,
1215 Bauer, S. E., Bellouin, N., Benedetti, A., Bergman, T., Berntsen, T. K., Beukes, J. P., Bian, H.,
1216 Carslaw, K. S., Chin, M., Curci, G., Diehl, T., Easter, R. C., Ghan, S. J., Gong, S. L., Hodzic, A.,
1217 Hoyle, C. R., Iversen, T., Jathar, S., Jimenez, J. L., Kaiser, J. W., Kirkevåg, A., Koch, D., Kokkola, H.,
1218 Lee, Y. H., Lin, G., Liu, X., Luo, G., Ma, X., Mann, G. W., Mihalopoulos, N., Morcrette, J.-J.,
1219 Müller, J.-F., Myhre, G., Myriokefalitakis, S., Ng, N. L., O'Donnell, D., Penner, J. E., Pozzoli, L.,
1220 Pringle, K. J., Russell, L. M., Schulz, M., Sciare, J., Seland, Ø., Shindell, D. T., Sillman, S.,
1221 Skeie, R. B., Spracklen, D., Stavrou, T., Steenrod, S. D., Takemura, T., Tiitta, P., Tilmes, S.,
1222 Tost, H., van Noije, T., van Zyl, P. G., von Salzen, K., Yu, F., Wang, Z., Wang, Z., Zaveri, R. A.,
1223 Zhang, H., Zhang, K., Zhang, Q., and Zhang, X.: The AeroCom evaluation and intercomparison of
1224 organic aerosol in global models, *Atmos. Chem. Phys.*, 14, 10845-10895, doi:10.5194/acp-14-10845-
1225 2014, 2014.

1226 Tsimpidi, A. P., Karydis, V. A., and Pandis, S. N.: Response of inorganic fine particulate matter to
1227 emission changes of sulfur dioxide and ammonia: The eastern United States as a case study, *Journal of*
1228 *the Air & Waste Management Association*, 57, 1489-1498, 2007.

1229 Tsimpidi, A. P., Karydis, V. A., and Pandis, S. N.: Response of Fine Particulate Matter to Emission
1230 Changes of Oxides of Nitrogen and-Anthropogenic Volatile Organic Compounds in the Eastern United
1231 States, *Journal of the Air & Waste Management Association*, 58, 1463-1473, 2008.

1232 Vieno, M., Heal, M. R., Twigg, M. M., MacKenzie, I. A., Braban, C. F., Lingard, J. J. N. Ritchie, S., Beck,
1233 R. C., A., M., Ots, R., DiMarco, C. F., Nemitz, E., Sutton, M. A., and Reis, S.: The UK particulate
1234 matter air pollution episode of March-April 2014: more than Saharan dust., *Environ. Res. Lett.*,
1235 doi:10.1088/1748-9326/11/4/044004, 2016.

1236 Walker, J. M., Philip, S., Martin, R. V., and Seinfeld, J. H.: Simulation of nitrate, sulfate, and ammonium
1237 aerosols over the United States, *Atmos. Chem. Phys.*, 12, 11213–11227, doi:10.5194/acp-12-11213-
1238 2012, 2012.

1239 Watanabe, S., T. Hajima, K. Sudo, T. Nagashima, T. Takemura, H. Okajima, *et al.* MIROC-ESM 2010:
1240 model description and basic results of CMIP5-20c3m experiments, *Geosci. Model Dev.*, 4 (2011), pp.
1241 845–872.

1242 Weber, R. J., Guo, H., Russell, A. G., and Nenes, A.: High aerosol acidity despite declining
1243 atmospheric sulfate concentrations over the past 15 years, *Nature Geosci.*, 9, 282-285,
1244 10.1038/ngeo2665, 2016.

1245 Williams, E. J., S. T. Sandholm, J. D. Bradshaw, J. S. Schendel, A. O. Langford, P. K. Quinn, P. J. LeBel,
1246 S. A. Vay, P. D. Roberts, R. B. Norton, B. A. Watkins, M. P. Buhr, D. D. Parrish, J. G. Calvert, and F.
1247 C. Fehsenfeld, An intercomparison of five ammonia measurement techniques, *J. Geophys. Res.*, Vol.,
1248 97, No. D11, Pages 11591-11611, July 20, 1992.

1249 van der Werf, G. R., Randerson, J. T., Giglio, L., Collatz, G. J., Mu, M., Kasibhatla, P. S., Morton, D. C.,
1250 DeFries, R. S., Jin, Y., and van Leeuwen, T. T.: Global fire emissions and the contribution of
1251 deforestation, savanna, forest, agricultural, and peat fires (1997–2009), *Atmos. Chem. Phys.*, 10,
1252 11707-11735, doi:10.5194/acp-10-11707-2010, 2010.

1253 Zender, C. S., Bian, H. S., and Newman, D.: Mineral Dust Entrainment and Deposition (DEAD) model:
1254 Description and 1990s dust climatology, *J. Geophys. Res.-Atmos.*, 108, 4416,
1255 doi:10.1029/2002jd002775, 2003.

1256 Zhou, J., B. Gu, W. H. Schlesinger, X. Ju, Significant accumulation of nitrate in Chinese semi-humid
1257 croplands, *Scientific Reports* 6, Article number: 25088, doi:10.1038/srep25088, 2016.

1258 **Table 1. Nitrate chemical mechanism and physical properties of AeroCom models**

| Model | CHEM-EQM | HNO ₃ chem mechanism | N ₂ O ₅ Hydrolysis | CHEM DUST | CHEM SEASALT | How do CHEMDUSS ^a | Bins for nitrate | Model Name & resolution | References |
|-------------|---|--|--|-----------|--------------|--------------------------------|---|-------------------------------|---------------------------|
| CHASER | ISORROPIA-I | CHASER (Sudo et al., 2002) | γ^b (0.1 for SO ₄ ²⁻ , NO ₃ ⁻ , OC, DU, and SS, and 0.05 for liquid cloud particles) (Dentener and Crutzen, 1993) | No | No | --- | Fine mode | MIROC, GCM, 2.8°x2.8°x64 | Watanabe et al., 2011 |
| EMAC | ISORROPIA-II (Stable state ^c) | MESSy2 (Jöckel et al., 2010) | γ (STA), STA ^d : climatological aerosol in Aitken, accumulation, and coarse soluble modes (Jöckel et al 2010). | Yes | Yes | ISORROPIA-II (TEQM) | 4 bins: Nucleation, Aitken, Accumulation, Coarse | ECHAM5, GCM, 2.8°x2.8°x31 | Karydis et al., 2016 |
| EMEP | MARS | EMEP EmChem09 (Simpson et al., 2012) | γ (STA, T, RH), STA: NH ₄ ⁺ , SO ₄ ²⁻ , NO ₃ ⁻ (Evans and Jacob, 2005; Davis et al., 2008) | Yes | Yes | First order loss (HETCHEM) | Fine and coarse | ECMWF-IFS, CTM, 0.5°x0.5°x20 | Simpson et al., 2012 |
| GMI | RPMARES (Stable state) | GMI (Straham et al., 2007) | γ (STA, T, RH), STA: BC, OC, SO ₄ ²⁻ , DU, SS (Evans and Jacob, 2005). | Yes | Yes | first order loss (HETCHEM) | 3 bins : (D<0.1, 0.1 - 2.5, > 2.5 um) | MERRA2, CTM, 2.5°x2.5°x72 | Bian et al., 2009 |
| INCA | INCA (Stable state) | INCA tropospheric chemistry (Hauglustaine et al., 2004) | γ (STA, T, RH), STA: BC, SO ₄ ²⁻ , DU, SS (Evans and Jacob, 2005). | Yes | Yes | first order loss (HETCHEM) | 2 bins : (D< 1µm and 1 - 10µm) | LMD-v4, GCM, 1.9°x3.75°x39 | Hauglustaine et al., 2014 |
| GISS MATRIX | ISORROPIA-II (Stable state) | MATRIX Bauer (2008) and tropospheric chemistry (Shindell et al., 2003) | γ (STA), STA: SO ₄ ²⁻ (Dentener and Crutzen, 1993) | No | No | NO | Distributed over all mixing states e.g. size distributions. | NASA GISS-E2, GCM, 2°x2.5°x40 | Schmidt et al 2014 |
| GISS OMA | EQSAM_v03d (Metastable ^e) | OMA (Bauer 2007) and tropospheric chemistry (Shindell et al., 2003) | γ (STA), STA: SO ₄ ²⁻ (Dentener and Crutzen, 1993) | Yes | No | Bauer and Koch, 2005 (HETCHEM) | Fine mode | NASA GISS-E2, GCM, 2°x2.5°x40 | Schmidt et al 2014 |
| Oslo CTM2 | EQSAM_v03d (Metastable) | Oslo CTM2 (Berntsen and Isaksen, 1997) | γ (STA), STA: climatology aerosol (Dentener and Crutzen, 1993; Søvdde et al., 2012). | No | Yes | EQSAM_v03d (TEQM) | 2 bins: fine and coarse mode | ECMWF, CTM, 2.8°x2.8°x60 | Myhre et al., 2006 |
| Oslo CTM3 | EQSAM_v03d (Metastable) | Oslo CTM2 (Berntsen and Isaksen, 1997) | γ (STA), STA: climatology aerosol (Dentener and Crutzen, 1993; Søvdde et al., 2012). | No | Yes | EQSAM_v03d (TEQM) | 2 bins: fine and coarse mode | ECMWF, CTM, 2.25°x2.25°x60 | Myhre et al., 2006 |

1259 ^aCHEMDUSS: Chemistry reaction on dust and sea salt particles

1260 ^b γ : the dimensionless uptake coefficient

1261 ^cStable state: where salts precipitate once the aqueous phase becomes saturated

1262 ^dSTA: Surface of Tropospheric Aerosols

1263 ^eMetastable: where the aerosol is composed only of a supersaturated aqueous phase

Formatted: Font color:

Formatted: Font color:

Formatted: Font color:

Formatted: Font color:

1264
1265
1266
1267
1268
1269
1270
1271
1272
1273
1274
1275
1276
1277
1278
1279
1280
1281
1282
1283
1284
1285
1286

Table 1. Nitrate chemical mechanism and physical properties of AeroCom models

| Model | CHEM-EQM | HNO3-chem mechanism | CHEM DUST | CHEM SEASALT | How-do CHEMDUSS | Bins-for nitrate | Model-Name & resolution | References |
|-------------|------------------------------|--|-----------|--------------|----------------------|---|-------------------------------|---------------------------|
| GHASER | ISORROPIA-I | GHASER (Sudo et al., 2002) | No | No | --- | Fine-mode | MIROC, GCM, 2.8°x2.8°x64 | Watanabe et al., 2011 |
| EMAC | ISORROPIA-II (Stable state*) | MESSy2 (Jöckel et al., 2010) | Yes | Yes | ISORROPIA-II | 4 bins: Nucleation, Aitken, Accumulation, Coarse | ECHAM5, GCM, 2.8°x2.8°x31 | Karydis et al., 2016 |
| EMEP | MARS | EMEP-EmChem09 (Simpson et al., 2012) | Yes | Yes | First-order loss | Fine and coarse | ECMWF-IFS, CTM, 0.5°x0.5°x20 | Simpson et al., 2012 |
| GMI | RPMARES (Stable state) | GMI (Straham et al., 2007) | Yes | Yes | first-order loss | 3 bins; (D<0.1, 0.1–2.5, > 2.5 µm) | MERRA2, CTM, 2.5°x2°x72 | Bian et al., 2009 |
| INCA | INCA (Stable state) | INCA-tropospheric chemistry (Hauglustaine et al., 2004) | Yes | Yes | first-order loss | 2 bins: (D< 1µm and 1–10µm) | LMD-v4, GCM, 1.9°x3.75°x39 | Hauglustaine et al., 2014 |
| GISS MATRIX | ISORROPIA-II (Stable state) | MATRIX-Bauer (2008) and tropospheric chemistry (Shindell et al., 2003) | No | No | NO | Distributed over all mixing states e.g. size distributions. | NASA-GISS-E2, GCM, 2°x2.5°x40 | Schmidt et al 2014 |
| GISS OMA | EQSAM_v03d (Metastable*) | OMA (Bauer 2007) and tropospheric chemistry (Shindell et al., 2003) | Yes | No | Bauer and Koch, 2005 | Fine-mode | NASA-GISS-E2, GCM, 2°x2.5°x40 | Schmidt et al 2014 |
| Oslo CTM2 | EQSAM_v03d (Metastable) | Oslo-CTM2 (Berntsen and Isaksen, 1997) | No | Yes | EQSAM_v03d | 2 bins: fine and coarse mode | ECMWF, CTM, 2.8°x2.8°x60 | Myhre et al., 2006 |

| | | | | | | | | |
|--------------|----------------------------|--|----|-----|------------|------------------------------------|-----------------------------------|-----------------------|
| Oslo CTM3 | EQSAM_v03d (Metastable) | Oslo-CTM2 (Berntsen and Isaksen, 1997) | No | Yes | EQSAM_v03d | 2-bins: fine and coarse mode | ECMWF, CTM, 2.25°x2.25°x6 0 | Myhre et al., 2006 |
|--------------|----------------------------|--|----|-----|------------|------------------------------------|-----------------------------------|-----------------------|

- 1287 ^aStable state: where salts precipitate once the aqueous phase becomes saturated
1288 ^bMetastable: where the aerosol is composed only of a supersaturated aqueous phase
1289 ^cCHEMDUSS: Chemistry reaction on dust and sea salt particles
1290
1291

Table 2. Characteristics of thermodynamic equilibrium models

| | ISORROPIA-I | ISORROPIA-II | MARS | RPMARES | INCA | EQSAM_v03d |
|--------------------------------------|---|--|---|---|---|---|
| Species | Sulfate, nitrate, ammonium, sodium, chloride | Sulfate, nitrate, ammonium, sodium, chloride, crustal species | Sulfate, nitrate, ammonium | Sulfate, nitrate, ammonium | Sulfate, nitrate, ammonium | Sulfate, nitrate, ammonium, sodium, chloride |
| # of components | 23 | 34 | 16 | 11 | 9 | 18 |
| # of reactions | 15 | 27 | 7 | 6 | 4 | 25 |
| Multicomponent activity coefficient | Bromley | Bromley | Bromley | Bromley | Seinfeld and Pandis | Metzger |
| Binary activity coefficient | Kusik and Meissner | Kusik and Meissner | Pitzer | Pitzer | Seinfeld and Pandis | Metzger |
| Water activity | ZSR ^a | ZSR | ZSR | ZSR | | ZSR |
| Kelvin effect | No | No | No | No | No | No |
| Quantities that determine subdomains | [Na ⁺], [NH ₄ ⁺], [SO ₄ ²⁻] | [Ca ²⁺], [K ⁺], [Mg ²⁺], [Na ⁺], [NH ₄ ⁺], [SO ₄ ²⁻] | RH, [NH ₄ ⁺], [SO ₄ ²⁻] | [NH ₄ ⁺], [SO ₄ ²⁻] | [NH ₄ ⁺], [SO ₄ ²⁻] | [NH ₄ ⁺], [SO ₄ ²⁻] |
| # of subdomains | 4 | 5 | 4 | 2 | 3 | 3 |

1292 ^aZSR: Zdanovskii-Stokes-Robinson
1293
1294

Table 3. Summary of the observational data used in this study

| SURFACE NETWORK | QUANTITY | COVER AREA | # of sites in 2008 | SAMPLE FREQUENCY | SOURCE |
|--------------------|---|----------------|--------------------|---------------------------------|--|
| CASTNET | Concentration of HNO ₃ , NO ₃ ⁻ , NH ₄ ⁺ , SO ₄ ²⁻ | North America | 83 | weekly | www.epa.gov/castnet/clearsession.do |
| | Dry deposition of them | | | | |
| AMoN | Concentration of NH ₃ | U.S. | 19 | 2-weekly | http://nadp.isws.illinois.edu/ |
| NADP/NTN | Wet deposition of HNO ₃ +NO ₃ ⁻ , NH ₄ ⁺ , SO ₄ ²⁻ | U.S. | 253 | weekly | nadp.isws.illinois.edu |
| EMEP | Concentration of HNO ₃ , NH ₃ , NO ₃ ⁻ , NH ₄ ⁺ , SO ₄ ²⁻ | Europe | 35 | daily | http://www.nilu.no/projects/ccc/index.html |
| EANET | Concentration of HNO ₃ , NH ₃ , NO ₃ ⁻ , NH ₄ ⁺ , SO ₄ ²⁻ | East Asia | 56 | Daily to 2-weekly | http://www.eanet.asia/eanet/brief.html |
| | Wet deposition of HNO ₃ +NO ₃ ⁻ , NH ₄ ⁺ , SO ₄ ²⁻ | | | 24 hours or precipitation event | |
| AIRCRAFT CAMPAIGNS | QUANTITY | COVER AREA | # of Flights | CAMPAIGN PERIOD | SOURCE |
| ARCTAS-A | Concentration of NO ₃ ⁻ , NH ₄ ⁺ , SO ₄ ²⁻ | Alaska, U.S. | 11 | March-April | http://www-air.larc.nasa.gov/cgi-bin/arcstat-c |
| ARCTAS-CARB | | California | 6 | June | |
| ARCTAS-B | | Bay area U.S. | 7 | July | |
| | | Central Canada | | | |

1295
1296
1297

Table 4a. NO₃⁻ global budget for each model

| Tracer | Model | Burden | SConc | DDep | WDep | ChemDUSS | ChemP ^a | Lifetime | AOD ^b |
|--------|-------|--------|-------|------|------|----------|--------------------|----------|------------------|
|--------|-------|--------|-------|------|------|----------|--------------------|----------|------------------|

| | | (Tg) | ($\mu\text{g kg}^{-1}$) | (Tg a ⁻¹) | (Tg a ⁻¹) | (Tg a ⁻¹) | (Tg a ⁻¹) | (Tg a ⁻¹) | (days) | |
|------------------------------|--------------------|------|---------------------------|-----------------------|-----------------------|-----------------------|-----------------------|-----------------------|--------|--------|
| NO ₃ ⁻ | CHASER | 0.16 | 0.18 | - | - | - | - | - | 0.0076 | |
| | EMAC | 0.67 | 0.47 | 46.3 | - | - | - | - | - | |
| | EMEP | 0.96 | 0.30 | 15.0 | 62.7 | | (71.7) ^c | 4.5 | 0.0073 | |
| | GISS-MATRIX | 0.22 | 0.06 | 1.3 | 9.6 | | (10.9) | 7.4 | - | |
| | GISS-OMA | 0.14 | 0.05 | 1.1 | 5.5 | | (6.6) | 7.8 | 0.0153 | |
| | GMI | 0.26 | 0.22 | 14.9 | 31.5 | 41.9 | | 4.8 | 2.1 | 0.0047 |
| | INCA | 0.79 | 0.17 | 4.5 | 44.6 | 44.1 | | 9.8 | 5.9 | 0.0064 |
| | Oslo-CTM2 | 0.60 | 0.25 | 47.8 | 61.5 | | (109.3) | | 2.0 | 0.0018 |
| | Oslo-CTM3 | 1.88 | 0.36 | 34.6 | 90.6 | | (125.2) | | 5.5 | - |
| | Avg | 0.63 | 0.23 | 20.7 | 45.9 | | 60.6 | | 5.0 | 0.0072 |
| | Med | 0.60 | 0.22 | 15.0 | 44.6 | | 46.7 | | 5.5 | 0.0064 |
| | Ratio ^d | 13.4 | 9.4 | 43.5 | 16.5 | | 19.0 | | 3.9 | 8.5 |

- 1298 | a: ChemP refers to NO₃⁻ chemical production associated with NH₃/NH₄⁺
1299 | b: AOD here includes NH₄⁺ that is associated to NO₃⁻ for all models except EMEP
1300 | c: value inside parenthesis is estimated total NO₃⁻ chemical production based on its
1301 | total loss, while budget without parenthesis is reported directly by model.
1302 | d: a ratio between maximum to minimum model simulations
1303 |
1304 |
1305 |

Table 4b NH₃ and NH₄⁺ global budget for each model

| Tracer | Model | Emi (Tg a ⁻¹) | Burden (Tg) | SConc ($\mu\text{g kg}^{-1}$) | DDep (Tg a ⁻¹) | WDep (Tg a ⁻¹) | ChemP/L ^a (Tg a ⁻¹) | Lifetime (days) | AOD |
|------------------------------|-----------------|---------------------------|-------------|---------------------------------|----------------------------|----------------------------|--|---------------------|--------|
| NH ₄ ⁺ | CHASER | | 0.75 | 0.44 | 20.9 | 7.2 | (28.1) ^b | 9.8 | - |
| | EMAC | | 0.19 | 0.12 | 3.6 | 44.5 ^c | - | - | - |
| | EMEP | | 0.20 | 0.15 | 4.0 | 26.4 | (30.4) | 2.4 | 0.0059 |
| | GISS-MATRIX | | 0.31 | 0.18 | 4.1 | 27.9 | (32.0) | 3.5 | - |
| | GISS-OMA | | 0.31 | 0.19 | 4.2 | 24.0 | (28.2) | 4.0 | - |
| | GMI | | 0.17 | 0.14 | 1.7 | 30.6 | 32.2 | 1.9 | - |
| | INCA | | 0.39 | 0.08 | 2.4 | 20.4 | 22.9 | 6.3 | - |
| | Oslo-CTM2 | | 0.29 | 0.14 | 5.3 | 32.6 | (37.9) | 2.8 | - |
| | Oslo-CTM3 | | 0.30 | 0.16 | 5.6 | 26.1 | (31.7) | 3.5 | - |
| | Avg | | 0.32 | 0.18 | 5.8 | 24.4 ^d | 30.4 | 4.3 | |
| | Med | | 0.30 | 0.15 | 4.1 | 26.3 ^d | 31.1 | 3.5 | |
| | Ratio | | 4.4 | 5.5 | 12.3 | 4.5 ^c | 1.7 | 5.2 | |
| | NH ₃ | CHASER | 62.8 | 0.13 | 0.46 | 19.8 | 6.8 | (36.2) ^b | 0.76 |
| EMAC | | 59.3 | 0.85 | 1.39 | 15.5 | - | - | - | |
| EMEP | | 56.9 | 0.09 | 0.46 | 15.4 | 18.2 | (33.6) | 0.98 | |
| GISS-MATRIX | | 63.4 ^e | 0.17 | 0.26 | 18.1 | 13.4 | (31.9) | 0.98 | |
| GISS-OMA | | 63.4 ^e | 0.17 | 0.25 | 18.4 | 16.7 | (28.3) | 0.98 | |
| GMI | | 60.4 | 0.11 | 0.40 | 12.6 | 17.5 | 30.4 | 0.67 | |
| INCA | | 70.5 ^e | 0.12 | 0.39 | 29.3 | 18.6 | 22.4 | 0.62 | |
| Oslo-CTM2 | | 65.9 | 0.08 | 0.27 | 15.8 | 8.1 | (42.0) | 0.44 | |
| Oslo-CTM3 | | 63.3 | 0.05 | 0.51 | 23.7 | 7.7 | (31.9) | 0.29 | |
| Avg | | 62.9 | 0.20 | 0.49 | 18.7 | 13.4 | 32.1 | 0.72 | |
| Med | | 63.3 | 0.12 | 0.40 | 18.1 | 15.1 | 31.9 | 0.72 | |
| Ratio | | 1.2 | 17.0 | 5.6 | 2.3 | 2.7 | 1.9 | 3.4 | |

1306 | ^aChemP/L: chemical production or loss term

1307 ^b chemical budgets inside parenthesis are inferred based on the reported emission
 1308 and total deposition

1309 ^c EMAC gives total wet deposition of NH₄⁺ and NH₃

1310 ^d Statistic values of NH₄⁺ wet deposition do not include EMAC

1311 ^e INCA uses ECLIPSE anthropogenic emissions, two GISS models use CMIP5
 1312 anthropogenic emission, and all other models use HTAPv2 anthropogenic emissions

1313

1314 **Table 4c. HNO₃ global budget for each model**

| Tracer | Model | Burden ^a (Tg) | SConc (µg kg ⁻¹) | DDep (Tg a ⁻¹) | WDep (Tg a ⁻¹) | CheAP ^b (Tg a ⁻¹) | CheGP ^c (Tg a ⁻¹) | CheAL ^d (Tg a ⁻¹) | CheGL ^e (Tg a ⁻¹) | Lifetime (days) |
|------------------|-----------------|-----------------------------|---------------------------------|-------------------------------|-------------------------------|---|---|---|---|--------------------|
| HNO ₃ | CHASER | 1.1 | 0.29 | 74.0 ^f | 120.9 ^f | - | - | - | - | - |
| | EMAC | 3.1 | 0.32 | 56.1 | 136.0 ^f | - | - | - | - | - |
| | EMEP | 0.66 | 0.04 | 39.2 | 123.9 | - | - | - | - | - |
| | GISS- MATRIX | 5.7 | 0.12 | 61.7 | 167.5 | - | - | - | - | - |
| | GISS- OMA | 5.3 | 0.10 | 49.8 | 148.2 | - | - | - | - | - |
| | GMI | 1.8 | 0.18 | 39.7 | 128.1 | 128.1 | 413 | 42.6 | 299 | 3.5 |
| | INCA | 1.5 | 0.09 | 47.7 | 77.5 | 21 | 369 | 10.0 | 210 | 5.7 |
| | Oslo- CTM2 | 1.3 | 0.05 | 36.1 | 66.0 | - | - | - | - | - |
| | Oslo- CTM3 | 2.3 | 0.04 | 36.0 | 49.3 | - | - | - | - | - |
| | Avg | 2.5 | 0.14 | 45.8 ^g | 108.7 ^g | - | - | - | - | - |
| | Med | 1.8 | 0.10 | 43.7 ^g | 123.9 ^g | - | - | - | - | - |
| Ratio | 8.6 | 8.0 | 1.6 ^b | 3.4 ^b | - | - | - | - | - | |

1315 ^aHNO₃ burden for the atmosphere up to 100 hPa

1316 ^bCheAP: chemistry production from aerosol phase

1317 ^cCheGP: chemistry production from gas phase

1318 ^dCheAL: chemistry loss from aerosol phase

1319 ^eCheGL: chemistry loss from gas phase

1320 ^ffor both HNO₃ and NO₃⁻

1321 ^gstatistical values do not include CHASER and EMAC that report total dry or wet
 1322 deposition of HNO₃ and NO₃⁻

1323

1324 **Table 4d. SO₄²⁻ global budget for each model**

| Tracer | Model | Emi SO ₂ (Tg a ⁻¹) | Emi SO ₄ (Tg a ⁻¹) | Burden (Tg) | SConc (µg kg ⁻¹) | DDep (Tg a ⁻¹) | WDep (Tg a ⁻¹) | Chem GP ^a (Tg a ⁻¹) | Chem AqP ^b (Tg a ⁻¹) | Lifetime (days) | AOD |
|-------------------------------|------------------|---|---|----------------|---------------------------------|-------------------------------|-------------------------------|--|---|--------------------|--------|
| SO ₄ ²⁻ | CHASER | 111 | 0 | 3.3 | 1.44 | 22.1 | 137 | (159) | 7.6 | 0.0826 | |
| | EMAC | 138 | 619 ^c | 1.9 | 1.72 | 504 ^d | 302 | (187) | 0.86 | - | |
| | EMEP | 109 | 0 | 0.83 | 0.45 | 10.2 | 109 | (119) | 2.5 | 0.0232 | |
| | GISS- MATRIX | 133 | 5.1 | 1.3 | 0.63 | 16.6 | 97 | (109) | 4.2 | - | |
| | GISS- OMA | 133 | 5.1 | 1.1 | 0.53 | 11.8 | 112 | 52.7 | 66.2 | 3.3 | 0.0714 |
| | GMI | 111 | 0 | 1.1 | 0.58 | 7.5 | 205 | 126.5 | 86.1 | 3.6 | 0.0257 |
| | INCA | 116 | 8.0 | 1.8 | 0.34 | 8.4 | 116 | 42.2 | 75.1 | 5.3 | 0.0417 |
| | Oslo- CTM2 | 133 | 4.1 | 2.0 | 0.49 | 17.6 | 184 | (198) | 3.6 | 0.0366 | |
| | Oslo- CTM3 | 133 | 4.1 | 2.7 | 0.55 | 20.2 | 160 | (176) | 5.5 | - | |
| | Avg ^e | 122 | - | 1.8 | 0.63 | 14.3 | 140 | - | 151 | 4.5 | 0.0469 |

| | | | | | | | | |
|--------------------|-----|-----|------|------|-----|-----|-----|--------|
| Med ^e | 133 | 1.6 | 0.54 | 14.2 | 127 | 139 | 3.9 | 0.0392 |
| Ratio ^e | 1.2 | 4.0 | 4.2 | 2.9 | 2.1 | 2.0 | 3.0 | 3.6 |

1325 ^a ChemGP: Chemistry production from gas phase reaction

1326 ^b ChemAqP: Chemistry production from aqueous phase reaction

1327 ^c EMAC emission also includes sea spray SO₄²⁻

1328 ^d EMAC dry deposition includes sedimentation and SO₄²⁻ sedimentation is very high
1329 since it has assumed that 7.7% of sea salt is SO₄²⁻

1330 ^d Statistical values do not include EMAC

1331

1332 **Table 5: Effective Henry Law constant used in the models**

| Aerocom Model | H ⁰ (M/atm) | -ΔH _{sol} /R (K) |
|-------------------|------------------------|---------------------------|
| CHASER | 3.0e+5 | 3400 |
| EMAC ^a | - | - |
| EMEP ^b | - | - |
| GIS MATRIX | 1.e+2 | 3415 |
| GISS OMA | 1.e+2 | 3415 |
| GMI | 1.05e6 | 4200 |
| INCA | 7.4e+1 | 3400 |
| Oslo-CTM2 | 3.3e+6 | 0 |
| Oslo-CTM3 | 3.3e+6 | 0 |

1333 ^aEMAC: See its wet deposition description in section 4.1.1.

1334 ^bEMEP: The model does not use Henry law but applies simple empirical scavenging
1335 ratio, which for NH₃ is 1.4e6 for in-cloud and 0.5e6 for below-cloud scavenging. The
1336 scavenging ratio by definition is the ratio the concentration of a certain pollutant in
1337 precipitation divided by the concentration of the pollutant in air.

1338

1339

1340

1341

1342

Table 6. Baseline and three sensitivity experiments in the GMI model

| Experiment | Setup | Purpose |
|------------|---|--|
| BASE | Standard simulation as described in section 2.1 | Baseline simulation |
| TWET | Set NH ₃ effective Henry law constant from 1.05e+6 (pH= 5.0) to 62 (pure water) | Review impact of NH ₃ wet deposition |
| TnoNH3 | Turn off NO ₃ ⁻ production from NH ₃ /NH ₄ ⁺ | Identify how large/where the NO ₃ ⁻ formation from NH ₃ /NH ₄ ⁺ |
| TnoHET | Turn off NO ₃ ⁻ production from dust and sea salt | Identify how large/where the NO ₃ ⁻ formation from dust and sea salt |

1343

1344 **Table 7: NO₃⁻, NH₄⁺, NH₃ and HNO₃ budgets from the base simulation and three**
1345 **sensitivity experiments**

| Tracer | Exps | Burden (Tg) | SConc (μg kg ⁻¹) | DDep (Tg a ⁻¹) | WDep (Tg a ⁻¹) | ChemDUSS (Tg a ⁻¹) | ChemP (Tg a ⁻¹) | Lifetime (days) |
|------------------------------|--------|-------------|------------------------------|----------------------------|----------------------------|--------------------------------|-----------------------------|-----------------|
| NO ₃ ⁻ | BASE | 0.26 | 0.22 | 14.9 | 31.5 | 41.9 | 4.8 | 2.1 |
| | Twet | 0.97 | 0.23 | 14.8 | 43.3 | 41.0 | 18.3 | 6.0 |
| | TnoNH3 | 0.20 | 0.17 | 14.7 | 27.5 | 42.3 | 0 | 1.7 |
| | TnoHET | 0.099 | 0.065 | 0.61 | 6.70 | 0 | 7.1 | 5.0 |

1346

| Tracer | Model | Emi | Burden | SConc | DDep | WDep | ChemP/L | Lifetime |
|--------|-------|-----|--------|-------|------|------|---------|----------|
|--------|-------|-----|--------|-------|------|------|---------|----------|

| | | (Tg a ⁻¹) | (Tg) | (µg kg ⁻¹) | (Tg a ⁻¹) | (Tg a ⁻¹) | (Tg a ⁻¹) | (days) |
|------------------------------|--------|-----------------------|------|------------------------|-----------------------|-----------------------|-----------------------|--------|
| NH ₄ ⁺ | BASE | | 0.17 | 0.14 | 1.7 | 30.6 | 32.2 | 1.9 |
| | Twet | | 0.48 | 0.16 | 1.9 | 50.7 | 53.0 | 3.4 |
| | TnoNH3 | | - | - | - | - | - | - |
| NH ₃ | BASE | 60.4 | 0.11 | 0.40 | 12.6 | 17.5 | 30.4 | 0.67 |
| | Twet | | 0.85 | 0.81 | 8.70 | 1.1 | 50.1 | 5.2 |
| | TnoNH3 | | 0.32 | 0.58 | 20.9 | 39.3 | 0 | 1.9 |
| | TnoHET | | 0.10 | 0.40 | 12.6 | 17.4 | 30.4 | 1.2 |

1347
1348
1349

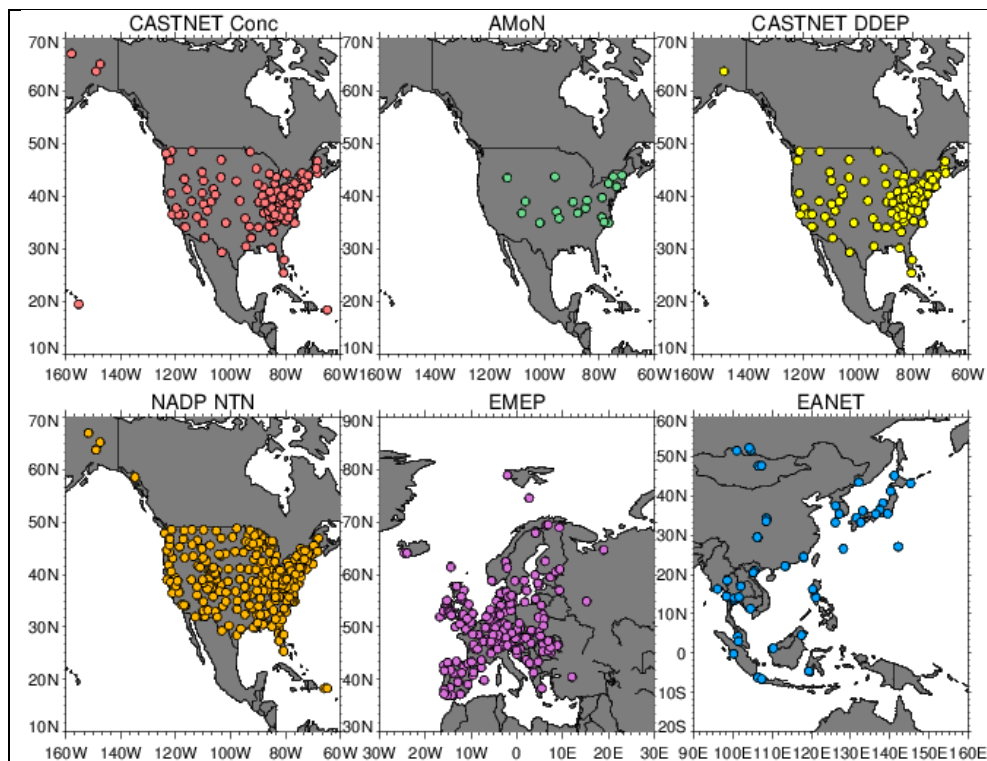


Figure 1. The observational station locations for CASTNET surface concentrations (CASTNET Conc), Ammonia surface monitor network over U.S. (AMON), CASTNET dry deposition (CASTNET DDEP); National Acid Deposition Network for wet deposition over U.S. (NADP NTN), surface concentrations over Europe (EMEP), and surface dry and wet deposition over Asia (EANET).

1350
1351
1352

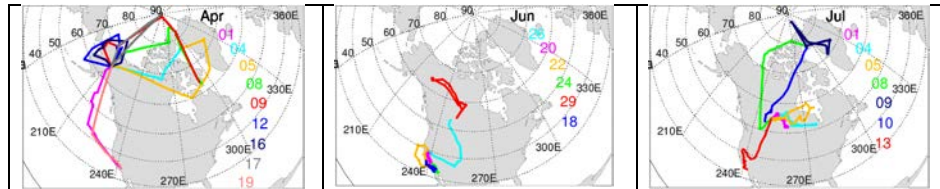


Figure 2. Flight-tracks of ARTCTA-A (left), ARCTAS-CARB (middle), and ARCTAS-B (right). The colors represent observations during different days.

1353